Marine Geology 467 (2024) 107185

Contents lists available at ScienceDirect

Marine Geology

journal homepage: www.elsevier.com/locate/margo

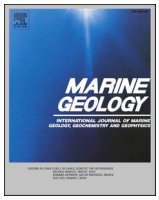

The infill of tunnel valleys in the central North Sea: Implications for sedimentary processes, geohazards, and ice-sheet dynamics

James D. Kirkham [a,b,*], Kelly A. Hogan [a], Robert D. Larter [a], Ed Self [c], Ken Games [c], Mads Huuse [d], Margaret A. Stewart [e], Dag Ottesen [f], Daniel P. Le Heron [g], Alex Lawrence [d], Ian Kane [d], Neil S. Arnold [b], Julian A. Dowdeswell [b]

[a] British Antarctic Survey, High Cross, Madingley Road, Cambridge CB3 0ET, UK
[b] Scott Polar Research Institute, University of Cambridge, Cambridge CB2 1ER, UK
[c] Gardline Limited, Hewett Road, Great Yarmouth NR31 0NN, UK
[d] Department of Earth and Environmental Sciences, University of Manchester, Manchester M13 9PL, UK
[e] British Geological Survey, The Lyell Centre, Research Avenue South, Edinburgh EH14 4AP, UK
[f] Geological Survey of Norway, P.O. Box 6315, Torgarden, N-7491 Trondheim, Norway
[g] Department für Geologie, Universität Wien, Josef-Holaubek-Platz 2, 1190 Wien, Austria

ARTICLE INFO

Editor: Michele Rebesco

Keywords:
Tunnel valley
3D seismic reflection data
Meltwater
Deglaciation
Ice sheets
North Sea

ABSTRACT

Tunnel valleys are widespread in formerly glaciated regions such as the North Sea and record sediment transport beneath ice sheets undergoing deglaciation. However, their complex infill architecture often makes their implications for ice-sheet processes difficult to unravel. Here, we use high resolution 3D (HR3D) seismic-reflection data, improved-resolution conventional 3D seismic-reflection data, and geotechnical information from industry-acquired boreholes to image the infill architecture of buried Quaternary tunnel valleys in the North Sea in unprecedented detail. Ten cross-cutting generations of tunnel valleys are mapped beneath the seafloor of the North Sea where only seven were visible previously. Each generation of tunnel valleys potentially reflects a different glaciation, although our evidence may imply that it is possible to rapidly erode and infill multiple generations of tunnel valleys within a single glacial cycle. The infill of the oldest tunnel valley generations reflects sedimentation during relatively gradual ice-sheet retreat, with occasional episodes of overriding by re-advancing grounded ice. Tunnel valleys formed in more recent glaciations are characterised by more variable sedimentation patterns that reflect dynamic fluctuations of the ice margin, including readvances and stagnation, during valley filling and ice retreat. Numerous subglacial landforms are also imaged within the tunnel valleys; these sometimes contain shallow gas accumulations that represent geohazards for seafloor infrastructure installations. In addition, we document examples where salt diapirism has caused fluids to migrate upwards from depth through faults and into the near-surface tunnel valleys. In instances where this occurs, the relatively porous and often highly continuous subglacial landforms present within their infill may allow these fluids to spread laterally for kilometres or even escape from the seafloor; it is therefore important to consider tunnel valleys when monitoring possible CO_2 leakage from carbon capture and storage efforts.

1. Introduction

Tunnel valleys represent a record of water flow, glacial erosion and sediment transport beneath ice sheets, particularly during deglacial phases. Obtaining a better understanding of the processes involved in tunnel valley formation is important as it may help to improve the parameterisation of melt rates, water routing and the interplay between basal hydrology and ice dynamics in numerical ice-sheet models under extreme melt conditions. Their location can also be used to reconstruct the position of former ice-sheet margins (e.g., Ehlers et al., 1984; Huuse and Lykke-Andersen, 2000b; Stewart et al., 2013). Tunnel valleys are important reservoirs of water, ore minerals and hydrocarbons; their variable infill can produce difficulties when interpreting seismic profiles of the subsurface (Kristensen and Huuse, 2012; Frahm et al., 2020; Warwel et al., 2022) and sometimes contains shallow gas accumulations which represent geohazards to drilling and increases the risks associated

* Corresponding author at: British Antarctic Survey, High Cross, Madingley Road, Cambridge CB3 0ET, UK.
E-mail address: jamkir56@bas.ac.uk (J.D. Kirkham).

https://doi.org/10.1016/j.margeo.2023.107185
Received 6 June 2023; Received in revised form 14 November 2023; Accepted 18 November 2023
Available online 25 November 2023

with installing seabed infrastructure (Lohrberg et al., 2020; Ottesen et al., 2020). In addition, the large dimensions of tunnel valleys (kilometres wide and hundreds of metres deep) allow them to capture potentially long-lived sedimentary successions that may otherwise be eroded or reworked by overriding glaciers on land, so they may contain valuable and potentially continuous records of sedimentary depositional history in otherwise poor preservation settings (Hepp et al., 2012; Huuse et al., 2012; Lang et al., 2012; Steinmetz et al., 2015; Coughlan et al., 2018). Obtaining a complete understanding of the processes responsible for tunnel valley formation is also important when planning the locations of deep geological repositories for nuclear waste in regions which may become glaciated again in the future (Iverson and Person, 2012; Beaud et al., 2016; Breuer et al., 2023).

Despite over a century of research, tunnel valleys remain relatively enigmatic glacial features because very few modern analogues for them exist beneath extant ice sheets. Whilst their geographical distribution and dimensions are relatively well known (van der Vegt et al., 2012; Ottesen et al., 2020), and recent advances have been made in understanding the manner and timescales over which tunnel valleys form (Beaud et al., 2018; Giglio et al., 2021; Kirkham et al., 2021; Kirkham et al., 2022), the processes responsible for their infilling remain poorly constrained. The age of tunnel valley infill deposits is also often difficult to assess due to reworking or a lack of datable material with which the age of the infill can be calculated (Ehlers and Linke, 1989; Praeg, 2003).

The internal infill lithologies and sedimentary architectures of tunnel valleys are notoriously complex as they can reflect a range of sedimentary and erosional processes that occurred during both glacial and post-glacial times (Kehew et al., 2012; Atkinson et al., 2013). Tunnel valley infill sequences are often separated into base (primary) and upper (secondary) fill units. The basal fill is typically glaciogenic in origin and often contains diamictons (Ehlers and Linke, 1989; van der Vegt et al., 2012) or massive gravels and sands which may have been deposited in a subglacial or ice-proximal setting (Ehlers and Linke, 1989; Ghienne and Deynoux, 1998; Le Heron et al., 2004). Secondary fill sequences are generally more varied and may comprise outwash fans and glaciofluvial deposits expelled at the margin of a receding ice sheet, or turbidity-current sequences deposited in proglacial lacustrine or marine environments (Ehlers et al., 1984; Ehlers and Linke, 1989; Janszen et al., 2012a; Kehew et al., 2012; Steinmetz et al., 2015). Laminated clays and silts deposited in more distal glaciomarine or glaciolacustrine environments are also commonly observed within the secondary fill sequence.

The infill of tunnel valleys is thus extremely diverse and varies according to the subglacial sedimentary processes active at that location, the amount and type of sediment load transported by the ice, and the interplay between ice movement, melting and grounding, as well as other post-glacial depositional processes. Genetic models of tunnel valley infill are therefore difficult to formulate in a manner which fulfils their diverse range of stratigraphic observations, and those which do exist often contrast. For example, van der Vegt et al. (2012) proposed a model in which the infill of tunnel valleys relates to their available accommodation space: smaller tunnel valleys are more likely to become entirely filled by glacial sediments, whereas larger valleys would be filled by sequences of ice-proximal followed by ice-distal sediments as the ice margin retreated away from the freshly cut channels. Other models attempt to explain the complex infill of tunnel valleys by multiple erosion and filling events, potentially beneath different ice sheets, with stagnant ice protecting portions of the valleys during retreat (Jørgensen and Sandersen, 2006); however, this model is less applicable in locations where clear upward fining sequences are evident. The lack of clarity about the processes involved in infilling tunnel valleys hinders their use as a resource to understand inaccessible subglacial processes operating beneath contemporary ice sheets, whilst the absence of a predictable infill model makes it difficult to plan for near-surface infrastructure installation in regions where tunnel valleys are present.

In this study, we exploit the wealth of high-resolution data from the North Sea — one of the most data-rich formerly glaciated environments on Earth — to quantify the complex patterns of tunnel valley infill in this region and explore their implications for ice-sheet processes, near-surface geohazards, and assess whether tunnel valleys need to be considered when monitoring potential leakage from carbon capture and storage efforts. We find that although the patterns of tunnel valley infill in this region are highly complex, the use of state-of-the-art high-resolution 3D (HR3D) seismic data permits a number of subtle patterns to be drawn out which inform about the processes of sedimentation beneath deglaciating ice sheets. Delicate subglacial landforms such as eskers and crevasse-squeeze ridges are imaged within the tunnel valleys and imply that tunnel valley formation is linked to dynamic ice-sheet behaviour in areas where meltwater production rates are high. These subglacial landforms may sometimes represent geohazards to seafloor infrastructure installations due to their ability to host shallow gas accumulations, and may impact carbon storage through creating imaging artefacts that complicate containment risk assessments and by creating preferential pathways through which escaped CO_2 could leak or escape through the seafloor. Our new data also reveals a number of new tunnel valley generations (10) which exceeds the maximum number mapped in previous studies (7). If, as previous studies have concluded, all of the tunnel valleys in the North Sea formed since Marine Isotope Stage 12 (MIS 12), our results indicate that more than one generation of tunnel valleys can form within a single glacial stage — pointing towards a more complex glacial history of western Europe than previously recognised.

2. Regional setting

The North Sea is a shallow epicontinental sea surrounded by the northwest European, Scandinavian and British landmasses with typical present-day water depths of ~30–150 m (excluding the Norwegian Channel, which is up to 700 m deep) (Fig. 1A). The North Sea Basin formed by lithospheric extension from the Paleozoic to Early Cretaceous (Ziegler, 1990, 1992) and contains up to three kilometres of sediments deposited throughout most of the Cenozoic Era (the last 65 Ma), including a sedimentary sequence up to 1000 m thick and ~ 140,000 km^3 in volume deposited during the Quaternary (2.6 Ma onwards) (Lamb et al., 2018; Ottesen et al., 2018). These sediments constitute a vast archive of past environmental conditions, including the build-up, advance and retreat of the Quaternary ice sheets around and into the basin (e.g., Cameron et al., 1987; Huuse and Lykke-Andersen, 2000b; Anell et al., 2012; Lamb et al., 2018; Ottesen et al., 2018; Rea et al., 2018).

The North Sea Basin has been glacially influenced discontinuously throughout most of the Quaternary (Ottesen et al., 2018). Evidence from sediment cores collected in the northern North Sea demonstrates that ice rafted debris transported by icebergs has been present since ~2.7 Ma (Eidvin and Rundberg, 2001; Ottesen et al., 2009), and iceberg ploughmarks have been imaged using seismic reflection data in buried surfaces dated to ~2 Ma in the central and southern part of the basin (Dowdeswell and Ottesen, 2013; Rea et al., 2018). Mega-scale glacial lineations, which are formed subglacially at the base of fast-flowing ice streams (e.g., Clark, 1993), have been observed in buried surfaces dating back to 1.87 Ma (Graham et al., 2010; Buckley, 2012; Rea et al., 2018); these lineations provide the earliest date that grounded ice could have advanced into the centre of the North Sea Basin.

During the early Quaternary, two largely independent depocentres developed in the northern and central-southern regions of the North Sea Basin. Fluvio-deltaic and pro-deltaic sediments derived from European and Scandinavian rivers infilled the southern sub-basin by around 1.6–1.7 Ma (Ottesen et al., 2014; Ottesen et al., 2018). The northern sub-basin of the early Quaternary North Sea Basin was infilled in a clockwise direction by prograding glacigenic debris-flows sourced from ice sheets on the Norwegian mainland (Ottesen et al., 2014; Batchelor et al., 2017; Ottesen et al., 2018; Løseth et al., 2020). Significant quantities of fluvio-deltaic sediment were also delivered to the northern sub-basin from the East Shetland Platform during this time (Batchelor et al., 2021). The

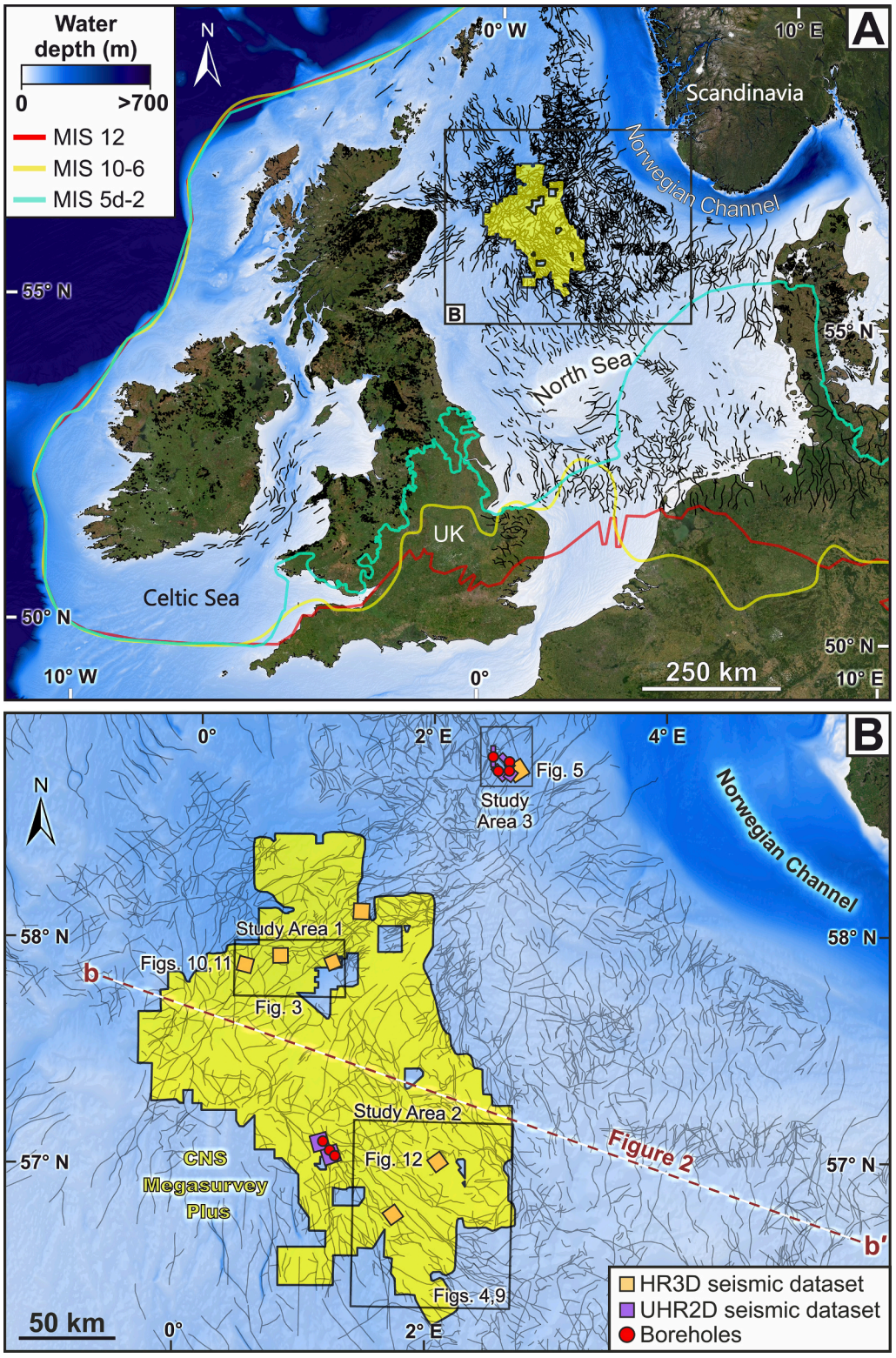

Fig. 1. Study area. (A) Distribution of tunnel valleys in the North Sea and surrounding landmasses (van der Vegt et al., 2012; Ottesen et al., 2020), and meltwater channels on the UK mainland (Clark et al., 2018). Best estimate former ice-margin positions for the Last Glacial Maximum (MIS 2), Saalian Glaciation (MIS 10–6), and Elsterian Glaciation (MIS 12) are shown from Batchelor et al. (2019). Regional bathymetry is from GEBCO (https://www.gebco.net). (B) Distribution of tunnel valleys in the central North Sea displaying the locations of the study areas examined in relation to the conventional 3D seismic data (PGS Central North Sea MegasurveyPlus; yellow polygon), high-resolution 3D seismic datasets (orange squares), ultra-high resolution 2D seismic datasets (purple squares), and boreholes (red circles) used in this study. The location of the regional 2D seismic line across the North Sea Basin displayed in Fig. 2 is shown. (For interpretation of the references to colour in this figure legend, the reader is referred to the web version of this article.)

deepest, central part of the North Sea Basin was the last area of the basin to be infilled and persisted until around 1 Ma (Ottesen et al., 2018; Løseth et al., 2022). The infilling of the North Sea Basin enabled the confluence of the Scandinavian and British-Irish ice sheets and encouraged the initiation of the Norwegian Channel Ice Stream at ~1–0.8 Ma (Sejrup et al., 1995; Ottesen et al., 2014; Batchelor et al., 2017), although recent seismic-stratigraphic evidence suggests that the Norwegian Channel Ice Stream may have initiated much later (~0.35 Ma) (Løseth et al., 2022). This major northward flowing ice stream eroded a significant proportion of the Early Pleistocene sediments deposited in the North Sea Basin, in addition to transporting large volumes of sediment eroded from terrestrial southern Norway and Sweden (Hjelstuen et al., 2012; Ottesen et al., 2016), and delivered a large amount of sediment to the North Sea trough-mouth fan, forming an Upper Regional Unconformity (URU) across much of the continental shelf (Nygård et al., 2005; Løseth et al., 2022) (Fig. 2).

Glacial influence in the central North Sea intensified around the time of the Middle Pleistocene Transition (~1 Ma) when the dominant orbital pacing of climate switched from the previously dominant 41 ka 'obliquity' cycle to the 100 ka 'eccentricity' cycle (Clark et al., 2006). This transition is recorded in the North Sea geological record by the substantial expansion of British-Irish and Scandinavian ice sheets into the North Sea Basin (Lee et al., 2012). However, the age and extent of many of these Middle Pleistocene glaciations remains ambiguous, particularly in the southern North Sea, due to the use of different approaches to construct relative stratigraphic frameworks, difficulties correlating stratigraphic models across national boundaries and between terrestrial and offshore records, and the limitations of geochronological methods (e.g., Ehlers et al., 1984; Laban, 1995; Vandenberghe, 2000; Clark et al., 2004; Rose, 2009; Lee et al., 2012).

Seismic stratigraphy correlated to ocean drilling records demonstrate that the Fennoscandian Ice Sheet advanced to the shelf break of the North Sea during MIS 14 (524–565 ka before present; BP), MIS 12 (~478–424 ka BP), MIS 10 (339–362 ka BP), MIS 6 (128–186 ka BP) and MIS 2 (~15–22 ka BP), and advanced to the inner shelf during MIS 8 (245–303 ka BP) (Dahlgren et al., 2002; Løseth et al., 2022). In contrast, the British-Irish Ice Sheet first expanded to the shelf edge in MIS 12, coalescing with the Fennoscandian Ice Sheet and advancing southward to reach a position close to the present-day coastlines of the Netherlands and East Anglia, UK (Fig. 1A). This glacial advance is documented in the North Sea by a widespread glacial erosion surface, tunnel valleys, and the infrequent presence of diamicton; similar geological markers also exist for MIS 12 within Denmark, the Netherlands, and Germany (Wingfield, 1990; Lang et al., 2012; Lee et al., 2012; Roskosch et al., 2015; Winsemann et al., 2020). Evidence for the expansion of the British-Irish Ice Sheet into the North Sea Basin during MIS 10 is more ambiguous, with differing chronological and stratigraphical interpretations proposed for the same data (Hamblin et al., 2005; Pawley et al., 2008; Rose, 2009). A similar maximum ice position to MIS 12 was attained during MIS 10–6, with regular shelf-edge expansions of the British-Irish and Fennoscandian ice masses along the European continental margin, the continued excavation of the Norwegian Channel by the Norwegian Channel Ice Stream, and the deposition of extensive glacial deposits and landforms in the southern North Sea (Ehlers, 1990; Sejrup et al., 1994; Sejrup et al., 1995; Nygård et al., 2005; Lee et al., 2012; Roskosch et al., 2015; Winsemann et al., 2020; Løseth et al., 2022). Ice was slightly less extensive during MIS 5d–2, extending only as far as northern Denmark and covering the southern central North Sea during the Last Glacial Maximum (MIS 2) (Ehlers, 1990; Ehlers and Wingfield, 1991).

Traditionally, discrete sets of tunnel valleys identified both onshore and incised into the relatively flat-lying middle to late Quaternary sediments offshore have been used to approximate former ice sheet extents and categorise the complex record of North Sea glacial history into three major glaciations: the Elsterian (MIS 12), the Saalian (MIS 10–6), and the Weichselian (MIS 5d–2) (Cameron et al., 1987; Wingfield, 1989, 1990; Ehlers and Wingfield, 1991; Praeg, 2003). In this three-stage glaciation model, the largest and most widespread tunnel valleys in the North Sea are generally associated with the Elsterian Glaciation, especially in the southern North Sea and adjacent land areas. Tunnel valleys are attributed to this time period based mainly on their large size, which may have been facilitated by the lack of stiff tills encountered by the ice as it advanced over the substrate for the first time (Passchier et al., 2010). These valleys are infilled with late Elsterian Lauenburg Clay and Holsteinian interglacial deposits, which are similar to deposits in other Elsterian tunnel valleys in Denmark and northern Germany (Huuse and Lykke-Andersen, 2000b). Just a few shallower tunnel valleys are interpreted to have been formed in MIS 10–6, mostly in the British and Dutch North Sea sectors of the North Sea, whilst tunnel valleys formed in MIS 5d–2 tend to be of intermediate size compared to the Saalian and Elsterian valleys, and are filled with sediments previously interpreted to have been deposited in a variety of environments ranging from high-energy fluvioglacial meltwater channels to quiet lacustrine or marine conditions (Huuse and Lykke-Andersen, 2000b; Kluiving et al., 2003; Lonergan et al., 2006; Stewart et al., 2012; van der Vegt et al., 2012; Steinmetz et al., 2015; Lang et al., 2018; Winsemann et al., 2020). However, the absolute ages of tunnel valleys in the North Sea are often highly uncertain due to a notable paucity of stratigraphic dating constraints, and increasing coverage and analysis of 3D seismic data in recent years has revealed considerably greater complexity in

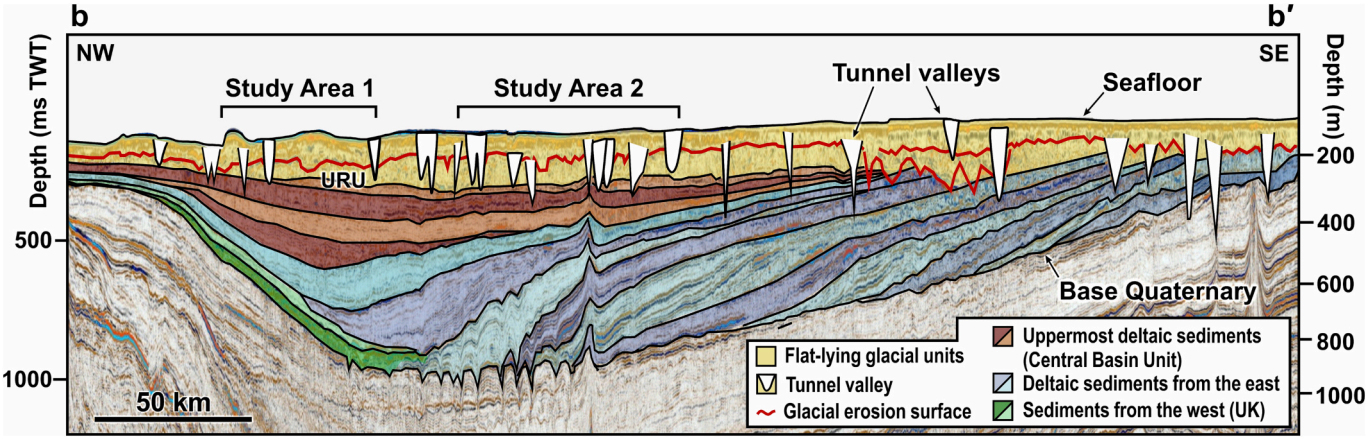

Fig. 2. Regional 2D seismic line across the North Sea Basin (NW–SE) showing the distribution of tunnel valleys within the Quaternary stratigraphy, provided by TGS. The locations of study areas 1 and 2 are shown. Image adapted from Ottesen et al. (2020), with location in Fig. 1B. URU — Upper Regional Unconformity. A velocity of 1800 m s^{-1} below the seafloor is used for depth conversion.

tunnel valley distribution than captured in earlier interpretations. For example, buried assemblages of tunnel valleys in the central North Sea can be separated into at least seven cross-cutting generations, each of which potentially reflects an individual glaciation (Stewart and Lonergan, 2011; Stewart et al., 2013; Ottesen et al., 2020), whilst tunnel valleys potentially spanning back to the Cromer Glaciation in MIS 16 (~676–621 ka BP) have been proposed in the southeastern North Sea (Lohrberg et al., 2022). This evidence has been used to argue that the traditional tripartite classification of North Sea glacial history is likely too simplistic.

3. Datasets and methods

The seismic data analysed in this study were collected using two classes of acquisition system with different horizontal and vertical resolutions. Small areas (typically between 1.5 and 40 km^2 per dataset) of HR3D seismic data were used to examine the infill architecture of buried tunnel valleys in unprecedented detail. A regional scale 3D seismic survey was then used to contextualise the HR3D seismic analysis and extend the interpretations of tunnel valley infill and architecture over a wider area.

3.1. High resolution 3D seismic data

Seven HR3D seismic datasets (Fig. 1B), covering a combined area of ~67 km^2, were used to conduct a detailed examination of the infill and internal architecture of the buried tunnel valleys. The acquisition system comprised two 1200-m-long streamers towed 3 m beneath the sea surface. The streamers had 96 hydrophone groups at 12.5 m spacing, a 6.25 m shot interval and a 1-ms sample rate. The seismic source consisted of two 4 × 40 in.^{3} (2.62 L) sleeve airgun clusters, fired in flip-flop formation, with a signal frequency range between ~20–250 Hz (Games, 2012). This acquisition system is particularly well suited for assessing the infill of shallow buried tunnel valleys as precise GPS positioning and laser tracking of the streamers permit data to be binned at a high resolution. In addition, the long length of the streamers enables velocity analyses to be conducted. The resulting velocity data can be used in a range of processes to suppress seismic multiples, which can be prominent in data from formerly glaciated continental shelves such as the North Sea (Games, 2012; Games and Wakefield, 2014; Games and Self, 2017). The final processed datasets consist of time-migrated 3D stacks with a 1-ms sample rate, a 6.25 × 6.25 m bin size and a vertical resolution of ~4 m, given the 100–125 Hz dominant frequency of the seismic-reflection data (Kallweit and Wood, 1982), and a detection limit for depth changes along individual reflectors of ~0.5 m (King, 2020; Kirkham et al., 2021). The final processed seismic data were analysed using S&P Global Kingdom Software.

3.2. Regional scale 3D seismic data

The HR3D seismic datasets are supplemented by the CNS MegaSurveyPlus, a merged regional scale 3D seismic dataset covering an area of 23,650 km^2 in the central North Sea produced by the marine geophysical company PGS. The CNS MegaSurveyPlus builds on areas where previous data coverage is already good by including legacy data from field tapes and data that is now of release age. These field data have been fully reprocessed in time and merged with previous data to provide better structural imaging and improved signal to noise ratios (PGS, 2020). The data consist of a 3D pre-stack time-migrated seismic cube that stretches ~200 km from north to south and ~ 140 km from east to west with a bin size of 12.5 × 12.5 m, although some data gaps are present (Fig. 1B). The vertical resolution of the MegaSurveyPlus is spatially variable owing to the different acquisition systems and conditions in which the merged data were surveyed; for the burial depths and regions examined here, the vertical resolution of the data is ~8–20 m. Regardless of these variations, the MegaSurveyPlus represents a significant improvement in both horizontal and vertical resolution over older regional scale 3D seismic surveys that have previously been used to study the morphology and infill of tunnel valleys (12.5–100 m bin size; e.g., Lonergan et al., 2006; Stewart and Lonergan, 2011; Stewart et al., 2013), including the previous version of the MegaSurvey (25 × 25 m bin size; Ottesen et al. (2020)).

Two sub-regions of the CNS MegaSurveyPlus were examined in detail in this study. These were chosen based on the locations of clusters of HR3D seismic data containing tunnel valleys which could be linked together using the regional scale 3D seismic survey. The first region, hereafter termed Study Area 1, comprises a 1500 km^2 area located in the central North Sea at the southern edge of the Witch Ground Basin at a latitude of ~58°N. Study Area 2 consists of a 7150 km^2 region located ~150 km southeast of Study Area 1 at a latitude of ~57°N (Fig. 1B), and contains the three longest tunnel valleys identified in the central and northern North Sea (Ottesen et al., 2020).

3.3. Geotechnical information from industry-acquired boreholes

In addition to the two regions of interest defined within the CNS MegaSurveyPlus, a third study area was chosen outside of the MegaSurveyPlus coverage in an area where a HR3D seismic dataset is accompanied by extensive ultra-high resolution 2D (UHR2D) seismic data (vertical resolution ~2 m) and several geotechnical boreholes which penetrated into and around several tunnel valley fills (Figs. 1B, S1). The CNS MegaSurveyPlus coverage does not extend this far north, so in this location we employ a lower resolution (25 × 25 m bin size) legacy 3D seismic dataset covering an area of 1466 km^2 to contextualise the tunnel valley observations (Fig. S1). The boreholes in and around the tunnel valleys reached depths of up to 100 m below the seafloor. Three tunnel valleys were sampled: Borehole 1 penetrated 76 m below the seafloor, 45 m of which recovered material from the tunnel valley (TV1) — approximately a fifth of its total depth. However, given the homogeneous seismic character of the infill facies, it is likely that the sediments sampled in Borehole 1 are representative throughout TV1. Borehole 2 reached a depth of 65 m below the seafloor, 15 m of which recovered material from within valley TV2, and Borehole 3 penetrated the flank of valley TV3 to a depth of 77 m below seafloor, sampling the upper 18 m of tunnel valley infill. Detailed geotechnical information were derived from the borehole samples, including material lithology, grain size, shear strength and water content; this information was used to aid interpretation of seismic facies and inform about the conditions in which the tunnel valleys in the region were infilled.

3.4. Mapping of buried tunnel valleys

An initial reconnaissance of tunnel valleys present in the HR3D seismic data was completed by examining sequential horizontal timeslices of the seismic volumes. These provide a planform 'map' of the buried tunnel valleys exposed at that depth of the timeslice (Lonergan et al., 2006). The high level of detail present in the HR3D seismic data then permitted the base and sides of each tunnel valley to be laterally traced through the 3D seismic volume and mapped as a horizon in seismic interpretation software. Once the general geometry of the tunnel valleys was established, the facies comprising their infill were examined. In a similar fashion to the base and sides of each valley, the top and base of each infill facies was digitised as an individual seismic horizon and then traced laterally in 3D through each of the HR3D seismic volumes. Any further surfaces, such as stratigraphic discontinuities, present inside the tunnel valley infill were also digitised and examined in 3D. The mapped seismic horizons were converted from two-way travel time (TWT) to depth using a velocity of 1900 m s^{-1} below the seafloor, which is appropriate for the Pleistocene sediments in this region (Kristensen and Huuse, 2012).

Elongate channels surrounding those observed in the HR3D data were mapped from the CNS MegaSurveyPlus using horizontal timeslices

at 20 ms intervals. The use of timeslice mapping can introduce artefacts into the data due to the arbitrary nature of 'cutting' through stratigraphic layering, especially if multiples are present in the data. Consequently, additional quality checks were used to confirm if each channel was a tunnel valley. These included whether the channel possessed distinctive morphological traits (such as abrupt terminations, steep side slopes) and if the channel thalweg (assessed using 2D vertical slices along the valley axis) undulated along the length of the valley. Once the regional mapping in the area surrounding the HR3D seismic datasets was complete, tunnel valleys were grouped into generations following the methodology of Stewart (2009). This workflow has been employed by numerous authors to map generations of buried tunnel valleys from 3D seismic data (e.g., Stewart and Lonergan, 2011; Stewart et al., 2013; Ottesen et al., 2020). In this method, tunnel valleys are assigned a relative age based on their crosscutting stratigraphic relationships and, if this is not well resolved or available, based on their orientation and stratigraphic depth (Stewart, 2009). This method permitted the tunnel valleys observed in the HR3D seismic datasets, and their infill architecture, to be placed into the regional context of tunnel valley generations and be given a relative age.

3.5. Examination of tunnel valley infill

The infill of each mapped tunnel valley was examined using vertical cross sections along their length at 100 m spacing for the CNS MegaSurveyPlus seismic data and at 25 m spacing for the HR3D seismic data. The infill of the tunnel valleys in Study Area 3 was not examined due to insufficient dataset resolution. Features of particular interest were examined at the highest possible resolution whilst seismic attributes, such as coherence, were also computed and analysed to help delineate internal structures within the tunnel valley infill. Horizontal timeslices were used to investigate how the seismic character of their infill varied spatially along the length of the tunnel valleys. For each of the tunnel valleys, the following information was assessed and recorded:

(i) The number of facies comprising the infill;
(ii) The detailed seismic character of each infill facies;
(iii) Whether any landforms (verified by 3D examination of their morphology along mapped seismic horizons) were present;
(iv) Whether the infill contained any evidence of deformation or thrust structures;
(v) Whether the infill contained any high-amplitude seismic reflections with additional characteristics such as phase-reversed polarity or acoustic masking of underlying reflectors, which may suggest the presence of shallow gas accumulations;
(vi) Whether the infill was internally confined or overtopped the valley shoulders.

4. Results

4.1. Mapped tunnel valleys

A total of 93 tunnel valleys were mapped in Study Area 1, and a further 228 were recorded in Study Area 2. Our revised mapping using high-resolution 3D seismic data reveals that tunnel valleys are spaced 2–4 times more densely than reported in previous studies (e.g., Lonergan et al., 2006; Stewart and Lonergan, 2011; Stewart et al., 2013; Ottesen et al., 2020). For example, 25 tunnel valleys had previously been mapped in the overlapping portion of Study Area 1 (16 mapped by Stewart, 2009; Stewart et al., 2013, later updated to 25 by Ottesen et al., 2020); this has now been revised to 75 tunnel valleys for the same area. Furthermore, subtle internal structures are visible within the tunnel valleys using HR3D seismic data — these have not been observed in previous investigations utilising lower-resolution 3D seismic data (Lonergan et al., 2006). The main increase in observed tunnel valley density is driven by the discovery of numerous smaller valleys that are difficult to detect confidently using lower resolution data. Accordingly, the greater number of tunnel valleys mapped here do not fit into the previous generational framework proposed by Stewart and Lonergan (2011). Instead, the tunnel valleys can be separated into 10 generations based on their cross-cutting relationships (Figs. 3 and 4).

Basic morphological parameters for the tunnel valley generations are similar to those previously described by Stewart et al. (2013) for the central North Sea. In Study Area 1, the tunnel valleys are 250–2100 m wide with width-to-depth ratios of 5–10. Generations 1, 2, 4, 5 and 10 are oriented southwest to northeast, whilst generations 3, 7, and 8 are broadly oriented north to south (Fig. 3A). Generations 6 and 9 are oriented southeast to northwest. Tunnel valleys in Study Area 2 are ~200–3800 m wide with average width-depth ratios of 6–8. Generations 1 and 3 are oriented southwest to northeast, whilst generations 2, 4, 5, 6, 8 and 10 are broadly orientated southeast to northwest (Fig. 4A). Generations 7 and 9 are orientated north to south. Four generations of tunnel valleys can be distinguished in Study Area 3. The valleys are 700–2000 m wide and are generally oriented north to south (Fig. S1). It is not clear whether the less complex pattern of tunnel valleys in this region is because of the lower seismic dataset resolution in Study Area 3 compared to the other regions, or if this observation reflects regional differences in tunnel valley incidence.

4.2. Tunnel valley infill

4.2.1. Seismic stratigraphy of tunnel valley infill facies

The systematic survey of 321 tunnel valleys imaged in the regional 3D and HR3D seismic data across study areas 1 and 2 reveals that seven types of infill are present (Fig. 6). Differences in the resolution of HR3D and conventional 3D seismic data result in some notable inconsistencies in the seismic character of tunnel valley infill in cases where the spatial coverage of these datasets overlaps. In Study Area 1, overlapping HR3D and conventional 3D seismic data coverage is present for tunnel valley generations 1–4, 6, 8, and 9, whilst overlapping seismic data coverage is present for generations 3, 5, 6, and 8 in Study Area 2.

The tunnel valleys present within the two study areas are characterised by three major infill facies (Figs. S2, S3). These three infill packages are commonly tens of metres thick and are capable of filling the valleys entirely (hundreds of metres thick). The first infill type consists of semi-continuous, sub-parallel reflections with low to medium amplitude that onlap onto the tunnel valley sides (Fig. 6). Type 1 infill is present in 64% of the tunnel valleys surveyed, and commonly comprises the main basal fill of the valleys. Smaller tunnel valleys can be entirely filled by this unit.

In contrast, Infill Type 2 consists of a homogeneous unit with low acoustic reflection amplitudes and a chaotic, mottled appearance that indicates very little internal structure at the resolution of the HR3D seismic data (Fig. 6). This facies is present in 31% of the tunnel valleys surveyed and can overtop the tunnel valley shoulders. In the regional 3D seismic data, these mottled reflections may merge together to form semi-continuous reflections that sometimes dip, potentially making it difficult to distinguish between infill types 1 and 2 using conventional 3D seismic data alone. Structures resembling clinoforms are sometimes visible within Infill Type 2 (Fig. S4); however, these are not as easily visible as previously recorded in tunnel valleys from other areas of the North Sea (Kristensen et al., 2008; Moreau and Huuse, 2014). In other profiles, this unit may appear completely transparent. Infill Type 2 is generally absent from the very smallest tunnel valleys and appears to be restricted to valleys that are larger than ~60 m deep and 250 m wide. This facies mostly comprises the upper fill unit in cases where multiple infill facies are present, and is rarely topped by a further seismic facies in the valleys. In instances where overtopping by a further unit does occur, Infill Type 2 tends to be overlain by infill types 1, 3, or 5. When Infill Type 2 is present in more complex fill sequences, it tends to comprise over half, and commonly over 70%, of the tunnel valley infill by volume. In rarer cases, this facies comprises the sole infill unit of the valley, especially in tunnel

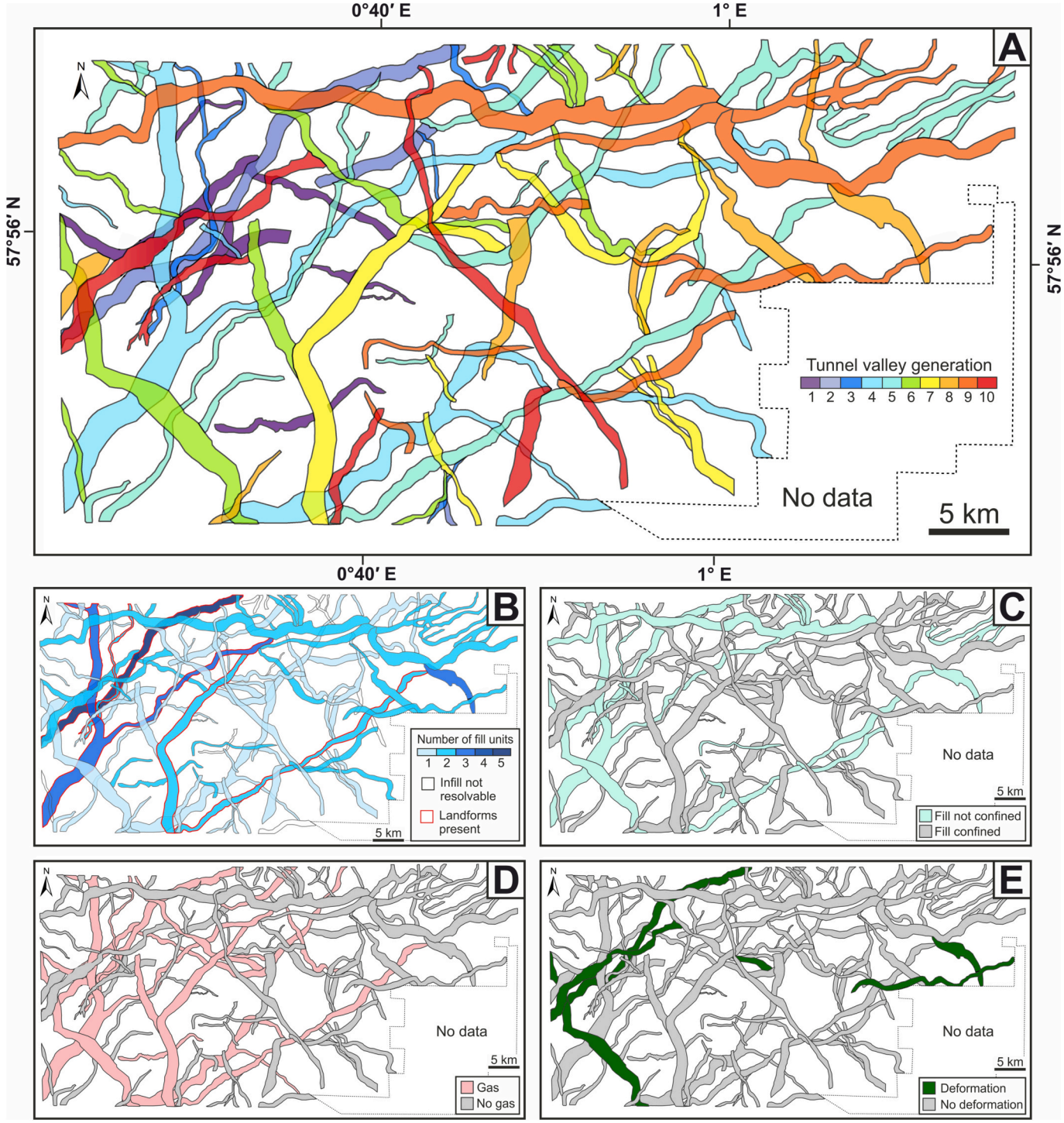

Fig. 3. Distribution and infill character of tunnel valleys in Study Area 1. (A) Tunnel valleys (mapped from 3D seismic timeslices) separated into ten generations based on their cross-cutting stratigraphic relationships, dominant orientation and stratigraphic depth. (B) Number of infill units and distribution of internal landforms (where present). (C) Map of infill which is confined to the tunnel valley sides or overtops the valley shoulders. (D) Presence of high-amplitude phase-reversed reflections signifying the presence of shallow gas. (E) Presence of deformed sediments comprising the tunnel valley infill.

valleys of smaller dimensions.

The third type of infill unit is characterised by medium amplitude concave reflections with high continuity that are sub-parallel to the valley floors. Infill Type 3 is present in 26% of the tunnel valleys surveyed and generally occurs within smaller valleys (<700 m wide, <125 m deep), either as the basal unit or as the only unit filling the valley. In tunnel valleys with multiple infill facies, this unit comprises only a small percentage (15–30%) of the valley cross-sectional area.

In addition to the three dominant infill facies, a further four infill types that are less widespread within the two study areas are also identified. Of these, the fourth type consists of medium amplitude stacked reflections that dip along the tunnel valley axis with angles of ~10–20° (Fig. 6). The reflections are only apparent from certain orientations and can therefore be difficult to detect, particularly in the regional 3D seismic data. This unit is up to several tens of metres thick.

The fifth infill type observed within the tunnel valleys is

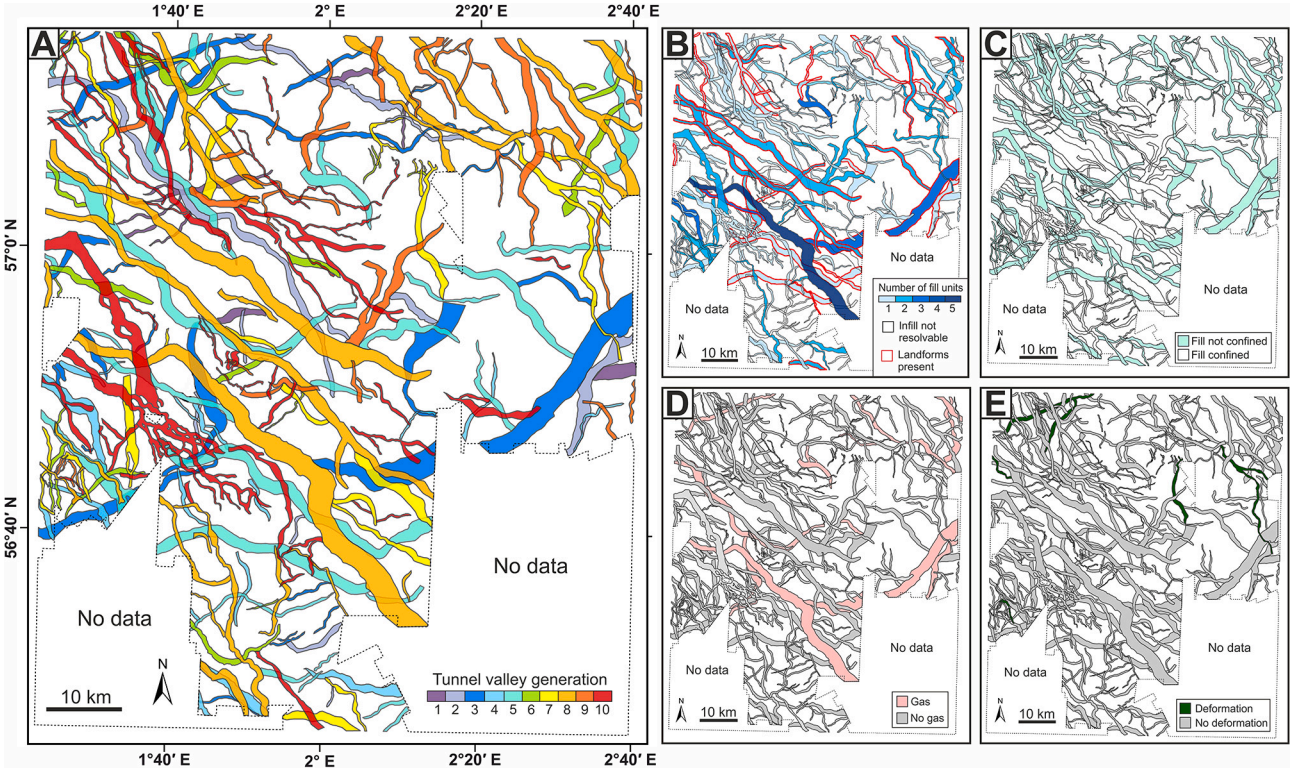

Fig. 4. Distribution and infill character of tunnel valleys in Study Area 2. (A) Tunnel valleys (mapped from 3D seismic timeslices) separated into ten generations based on their cross-cutting stratigraphic relationships, dominant orientation and stratigraphic depth. (B) Number of infill units and distribution of internal landforms (where present). (C) Map of infill which is confined to the tunnel valley sides or overtops the valley shoulders. (D) Presence of high-amplitude phase-reversed reflections signifying the presence of shallow gas. (E) Presence of deformed sediments comprising the tunnel valley infill.

characterised by thick sequences of stratified continuous low-medium amplitude parallel reflections that have high continuity. When present, Infill Type 5 generally occurs at the top of the valley fill sequence. This infill unit is most commonly observed within larger tunnel valleys, although it may be difficult to distinguish between Type 5 and Type 2 deposits using conventional 3D seismic data alone due to their similar appearance at coarser resolutions.

Infill Type 6 is comprised of large blocks of high amplitude chaotic reflections or steep (10–42°) breaks in otherwise continuous parallel reflections that run along the tunnel valley sides. When present, this unit can comprise ~10–30% of the tunnel valley infill by volume. The final infill class (Type 7) consists of discontinuous blocks of very high amplitude semi-disrupted reflections that are sometimes found at the base of the tunnel valleys. The thickness of this unit is typically small (<10s m) compared with the depth of the tunnel valleys in which it is found (100s m).

4.2.2. *Landforms buried within tunnel valleys*

Previous analysis of HR3D seismic data demonstrates that over 40% of tunnel valleys in the central North Sea contain smaller glacial landforms buried within the valleys (Kirkham et al., 2021). The dimensions of many of these landforms — particularly kettle holes, braided channel structures, and crevasse-squeeze ridges — are below the detection limit of conventional 3D seismic data and can only be imaged within the small spatial extent of the HR3D seismic datasets. However, further analysis over a larger spatial scale using conventional 3D seismic data confirms that many additional tunnel valleys outside the confines of the HR3D seismic data contain high-amplitude reflections between their difference infill facies (Fig. 9). These reflections can largely be distinguished using conventional 3D seismic data due to their high degree of continuity (e.g., Fig. 9A) and their association with shallow gas-bearing deposits (Fig. 9E). When mapped in 3D, these high-amplitude reflections delineate sinuous ridges that are up to 14 km long, 30–150 m wide, and 5 m high on average (Fig. 9A, B), as well as crudely streamlined island-like features that are up to 1 km long and 300 m wide (Fig. 9C, D). We interpret the ridges as eskers that were deposited in meltwater conduits present at the base of an ice sheet (Kirkham et al., 2021), and the island-like features as mega-rafts deposited by glacitectonic processes (e.g., Janszen et al., 2012a; Evans et al., 2020).

4.2.3. *The infill of different tunnel valley generations*

The tunnel valleys mapped in study areas 1 and 2 contain 1–5 infill facies (Figs. 3, 4, 8). The majority of tunnel valleys are characterised by 1–2 seismic facies, although this is likely at least partially related to the resolution of the seismic data, as tunnel valleys covered by the higher resolution HR3D seismic data typically contain a greater number of seismic facies than the surrounding valleys surveyed by the MegaSurveyPlus (Figs. 3B, 4B). Larger (both deeper and wider) tunnel valleys generally contain more fill units, although many relatively wide valleys are also characterised by only 1–2 seismic facies.

Type 1 infill constitutes the most widespread facies observed, with at least one tunnel valley within each generation containing this unit. Type 2 infill is the second most widespread (6 out of 10 generations), whilst four generations contain Type 3 infill. Rarely, small units of Type 7 infill are present discontinuously along the base of some tunnel valleys, although it is difficult to confidently image these units without the greater resolution of the HR3D seismic data.

Although tunnel valleys in generations 1–4 contain up to 4 seismic facies, the majority are dominated by a single unit of Type 1 infill. This unit is typically unconfined by the valley sides and occasionally contains remnant landforms (Section 5.2.2), phase-reversed reflections indicative of gas-bearing deposits, and some evidence of deformation or imbricated reflections. A few tunnel valleys are also filled with concave (Type 3) or chaotic (Type 2) reflections, with the latter not confined by the valley

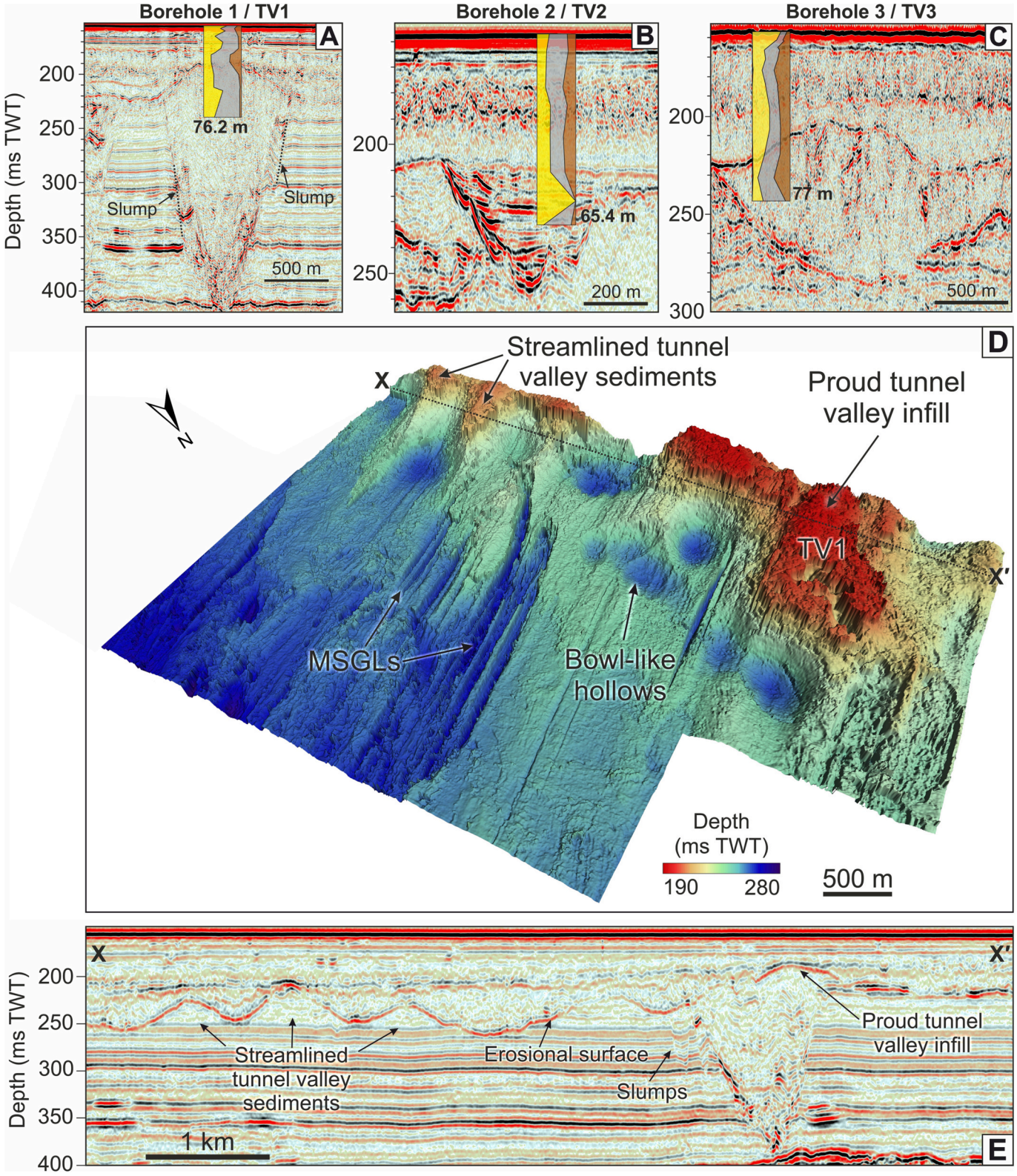

Fig. 5. Geotechnical boreholes in Study Area 3. (A, B, C) Ultra-high resolution 2D seismic data displaying the tunnel valleys sampled by geotechnical Boreholes 1–3. Borehole colours represent the relative concentration of sands, silts and clay throughout the length of the boreholes (sand = yellow, silt = grey, clay = brown). See Fig. S1 for borehole locations. (D) Erosional surface over the top of Tunnel Valley 1 (TV1) mapped from high resolution 3D seismic data. The surface contains a proud-standing tunnel valley infill and streamlined subglacial landforms including megascale glacial lineations and features resembling crag-and-tails. (E) High resolution 3D seismic section along the length of the mapped surface displaying the proud tunnel valley infill. (For interpretation of the references to colour in this figure legend, the reader is referred to the web version of this article.)

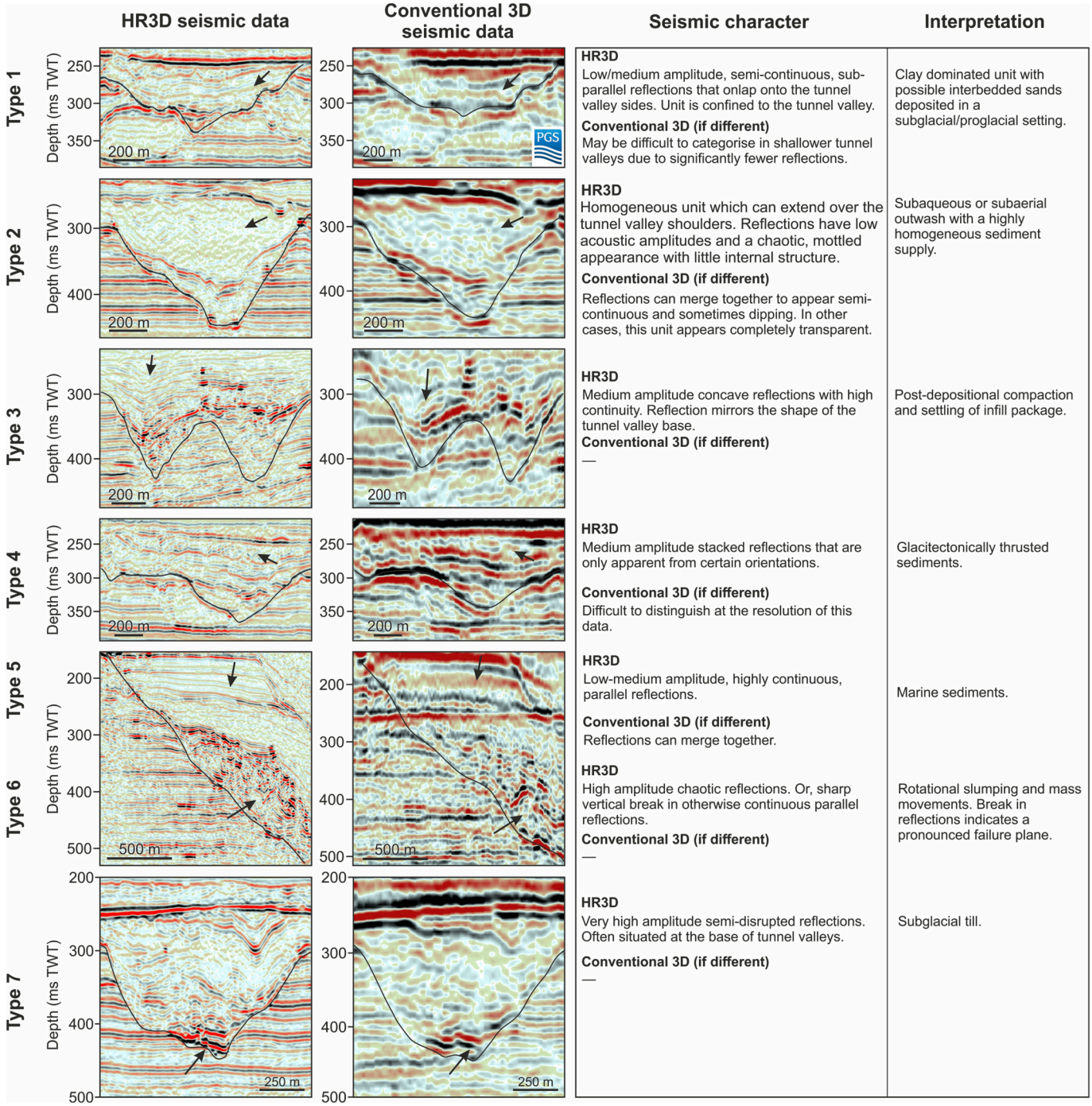

Fig. 6. Seismic facies identified within the infill of central North Sea tunnel valleys. Differences in seismic character are sometimes present between the high-resolution 3D (HR3D) seismic data and the conventional 3D seismic data. Arrows highlight the infill type. TWT — two-way travel time.

sides and sometimes burying the Type 1 unit that commonly fills the base of the valleys.

Generation 5 contains a highly consistent fill pattern of either a 1–2 units of Type 1 infill that occasionally contains landforms and gas-bearing deposits, or concave Type 3 reflections at the valley base capped by a unit of Type 2 infill that consistently overflows the valley sides. Generation 5 valleys consist mostly of two seismic facies but can contain 1–3 fill units. Landforms and gas-bearing deposits occur at a higher frequency within generation 5 tunnel valleys than in other generations, especially within Study Area 2. These features are mostly associated with Type 1 infill.

Generations 6–8 tunnel valleys are mostly comprised of 1–2 units of Type 1 or Type 3 infill, with occasional instances of Type 2 fill. In cases where valleys contain two seismic facies, the upper unit is comprised of Type 1 or Type 2 infill. Where present, the Infill Type 2 frequently overtops the valley shoulders. Deformed sedimentary structures and landforms, including eskers and island-like blocks, are relatively common within generation 8 tunnel valleys (Fig. 9) — particularly those associated with Type 1 infill deposits. Within Study Area 2, generation 8 contains a massive tunnel valley that is the longest documented in the North Sea (155 km; Ottesen et al., 2020). With the addition of the revised regional-scale 3D seismic data, our mappings extend the length of this tunnel valley to over 195 km, making it the longest tunnel valley documented anywhere in the world. The tunnel valley is ~360 m deep

and contains 5 seismic facies. The lower three facies consist of packages of Type 1 infill that contains gas-bearing deposits. These are capped by a unit of Type 2 infill, and finally a drape of Type 5 infill.

The generation 9 tunnel valleys are largely infilled with a single unit dominated by Type 1 sediments, although infill types 2 and 3 are also present in some valleys. Eskers (Fig. 9A, B) and crudely streamlined island-like features that are up to 1 km long and 300 m wide (Fig. 9C, D) are observed within some tunnel valleys, visible as high-amplitude reflections commonly present within Infill Type 1. The infill of many tunnel valleys of this generation is unconfined. Finally, the infill of generation 10 is comprised of a single unit of Type 1 or Type 3 fill. Landforms are absent from the valley fills and ~ 50% of the fill is unconfined. Most tunnel valleys in this generation contain only one fill unit.

4.2.4. Geotechnical borehole information

Geotechnical information was analysed for six boreholes in Study Area 3. Three boreholes sampled the infill of distinct tunnel valleys in this region (termed TV1, TV2 and TV3) and the remainder sampled the substrate immediately adjacent to the channels. The three tunnel valleys are of intermediate size compared to others in our updated inventory.

TV1 is 950 m wide, 234 m deep and has a distinctive V-shaped morphometry. In the HR3D seismic data, the infill of TV1 is dominated by low amplitude chaotic reflections with a mottled appearance (Infill Type 2) which are extensively faulted along flanks of the valley (Fig. 5A). These faults correspond to pervasive slumping of large sediment blocks which fill the valley base (Kirkham et al., 2021), forming glacial curvilineations along the crest of the scarps (Kirkham et al., 2022). The top of the tunnel valley infill is notable as it exhibits a domed upper surface which stands proud of the valley shoulders by ~30 m (Fig. 5A). Tracing the reflection corresponding to the top of the tunnel valley into adjacent areas reveals the presence of streamlined glacial landforms indicative of overriding by a fast-flowing grounded ice sheet (Fig. 5D); this fast ice flow appears to have differentially eroded the infill of the tunnel valleys in this region, with the softer sediments surrounding the infilled valley being preferentially eroded (Fig. 5E).

Borehole 1 suggests that the infill of TV1 consists of coarse silts and fine sands that are sometimes interbedded with thick layers of coarse silt. Corrected cone penetration tests reveal that the sediments are very dense, with cone resistance values of up to 90 MPa. The proportion of clay within the tunnel valley fill (~4%) is greatly diminished compared to adjacent sediments into which TV1 is incised (typically 30–60%). Instead, this fraction of clays is replaced with higher proportions of fine sands (+10–20%) and coarse silts (+10–30%) relative to the surrounding substrate at similar depths. Gravel-sized sediments are also absent from TV1 despite small proportions being present in the boreholes surrounding the tunnel valley which were probably deposited by ice rafting.

TV2 is 600 m wide and 55 m deep. When imaged using UHR2D seismic data, the valley infill is characterised by medium to high amplitude semi-continuous reflections that onlap the valley sides (Type 1 infill) (Fig. 5B). Geotechnical information from Borehole 2 reveals a greater degree of variability compared to Borehole 1. Samples range from very dense fine sands (100% of sample), which correspond to the higher amplitude reflections within the valley, to coarse silts (72% of sample) with smaller percentages of sands and clays (16% and 12%, respectively). Gravel is completely absent from the infill of TV2, yet small percentages are present in the surrounding substrate, probably deposited by ice rafting. The lithology of the infill of TV2 is relatively similar to neighbouring boreholes located outside of the valley but with slightly higher proportions of silt than the surrounding boreholes. Borehole 2 also lacks the thin laminae and beads of clays and silts that are common in other boreholes surrounding TV2.

TV3 is ~1300 m wide, up to 72 m deep and exhibits a domed upper surface similar to TV1. The UHR2D seismic data reveals that the infill of TV3 consists of low amplitude chaotic seismic reflections with little internal structure (Type 2 infill), although some isolated high amplitude reflections are present within the central upper portion of the valley infill (Fig. 5C). Material recovered from Borehole 3 demonstrates that TV3 is infilled by silts (43–59%) and clays (11–42%) which sometimes contain fractions of fine sand. The valley infill contains a lower fraction of fine sands (13–29%) than the other valleys sampled.

5. Discussion

5.1. Interpretation of tunnel valley infill facies

Three major units (infill types 1–3) dominate the infill of the central North Sea tunnel valleys. Geotechnical information from Infill Type 1 (Borehole 2) demonstrates that the onlapping sub-parallel reflections characteristic of this facies reflect sedimentary layers consisting of varying fractions of fine sands and coarse silts. These lithological variations would produce more acoustic contrasts and therefore may explain the strong and continuous character of the seismic reflectors associated with this unit. Infill Type 1 can also contain medium to high amplitude reflections that correspond to subglacial landforms (see Kirkham et al., 2021) buried within or at the upper boundary of this unit, or deformation within the unit itself. Based on these characteristics, we interpret Infill Type 1 as reflecting ice-proximal sedimentation close to the ice-sheet grounding zone.

A similar facies to Infill Type 1, described as massive to cross-bedded in structure, is observed along the floors of many Late Ordovician tunnel valleys in northern Africa and Arabia (Fig. 7A–C) (Le Heron et al., 2004; Clerc et al., 2013). This unit can be up to 40 m thick, although its thickness varies along the length of the valley. Clerc et al. (2013) suggest that this sedimentary facies was deposited rapidly from granule-rich, high-density turbulent underflow currents expelled from beneath a lightly grounded ice sheet. Deposition of the coarser fraction of the sediment carried by this meltwater would have occurred close to the outlet whilst finer sands, silts, and clays would be carried further in rising meltwater plumes and rain out from suspension further from the outlet (Syvitski, 1989; Mugford and Dowdeswell, 2011; Dowdeswell et al., 2015). These glacimarine deposits sometimes contain evidence for deformation, recording the occasional re-grounding of the ice sheet upon these sediments within the partially grounded zone (Clerc et al., 2013). A further similarity between Late Ordovician examples of tunnel valleys and those in the North Sea is the presence of deformation of the unit into which the tunnel valleys are incised at the sides of the erosional unconformity (Fig. 7D). The observed side wall deformation potentially reflects a combination of ice loading in conjunction with probable sediment piping through the conduit during tunnel valley formation (Le Heron et al., 2004).

Samples from Borehole 1 (Fig. 5A) demonstrate that the mottled seismic reflections characteristic of Infill Type 2 correspond to very dense homogeneous silty sand with a low clay content. We interpret Infill Type 2 as subaqueous or subaerial proglacial outwash with a highly homogeneous sediment supply. The morphological, geophysical, and geotechnical characteristics of this unit are similar to upper valley fill deposits recorded in late Ordovician examples of tunnel valleys in northern Africa which feature well-sorted, fine-to coarse-grained sandstones with limited grain size variations that can extend over the valley shoulders (Fig. 7) (Le Heron et al., 2004; Clerc et al., 2013). Clinoform-like geometries are sometimes recognised within this unit, and small-scale sedimentary structures such as planar lamination, primary current lineations, convolute lamination, rare antidune stratification, current ripple cross-lamination and largescale undulose bedding have also been observed (Le Heron et al., 2004; Clerc et al., 2013). An absence of glaciotectonic deformation structures suggests that there was no ice contact during the time that this unit was deposited (Clerc et al., 2013). When viewed from a regional perspective, these massive cross-bedded sandstones form a regionally extensive blanket which extends for tens of kilometres and can be several tens of metres thick (Girard et al., 2012;

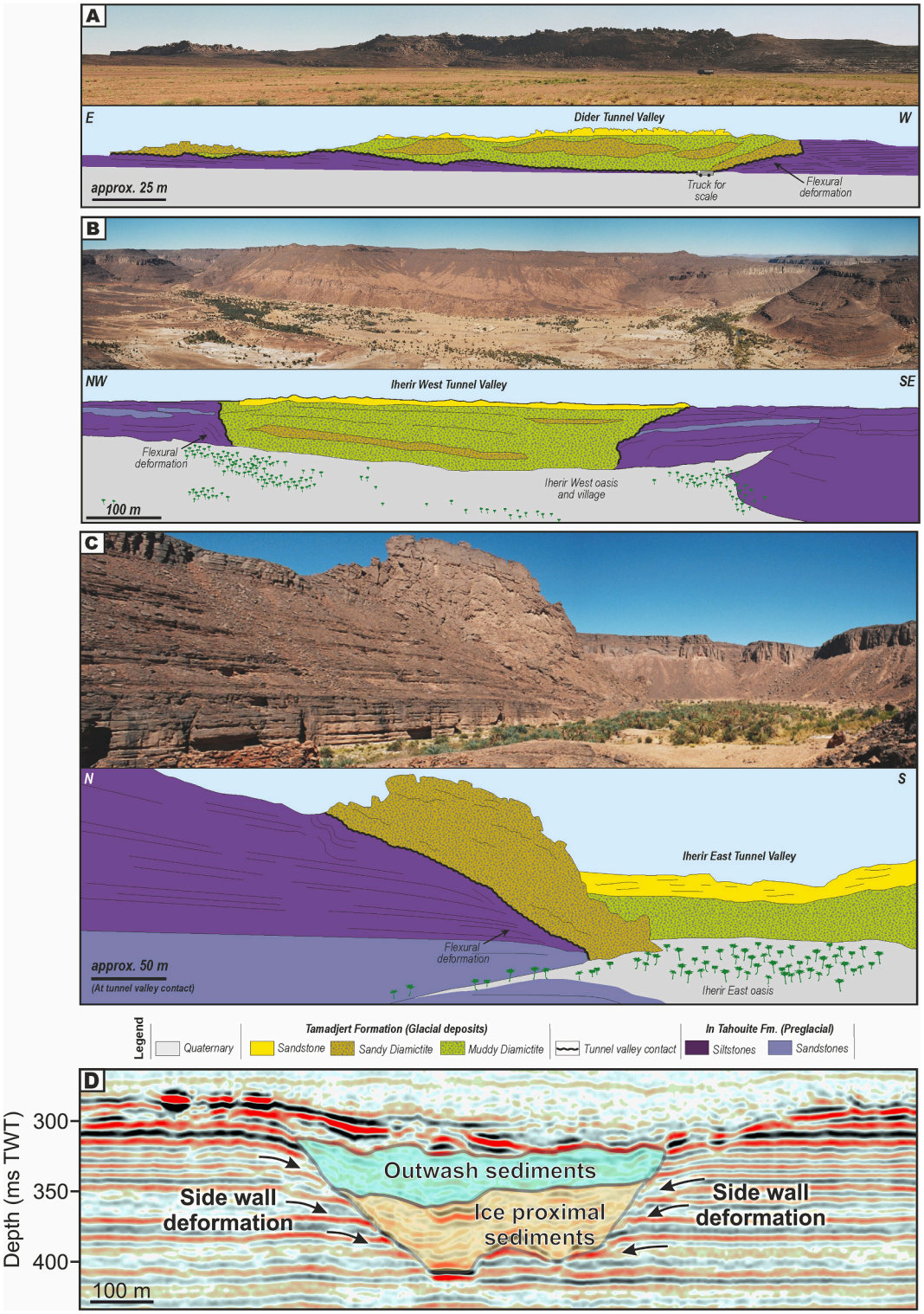

Fig. 7. Examples of Late Ordovician tunnel valleys in the Tassili N'Ajjer region of Algeria together with interpretative sketches of their geometry and architecture. (A) The Dider palaeovalley, located at 25° 8′ 52.313″ N, 8° 30′ 1.919″ E. A truck near the outcrop provides an approximate scale. (B) The Iherir West structure (25° 23.832′N, 8° 24.974′E) — small buildings in the valley provide an approximate scale. (C) The Iherir East locality (25° 25.487′N, 8° 25.743′E), with scale applicable to the nearfield to the left of the image. In (A) and (B) the entire cross-section of the tunnel valley is shown; in (C) only one margin is visible. Note that in all cases evidence for deformation in strata immediately underlying the glacial deposits is observed, interpreted to originate through with loading from an overlying ice mass as the tunnel valley developed. (D) Example tunnel valley from the central North Sea displaying similar infill architecture and side wall deformation as the Late Ordovician examples in (A–C).

Hirst et al., 2012). This sedimentary unit has been interpreted as proglacial or glacimarine outwash deposited beyond the grounding zone during temporary stillstands punctuating a final relatively rapid retreat of the marine-terminating ice-sheet margin (Clerc et al., 2013; Dowdeswell et al., 2015).

Infill Type 3 does not contain landforms or shallow gas deposits and is commonly confined to the valley sides. We interpret Infill Type 3 to represent post-depositional deformation of the infill package driven by factors such as porosity changes or sediment compaction. In some cases, this unit is associated with salt domes that underlay the tunnel valleys — particularly in the southern central North Sea. However, this association does not apply to all tunnel valleys.

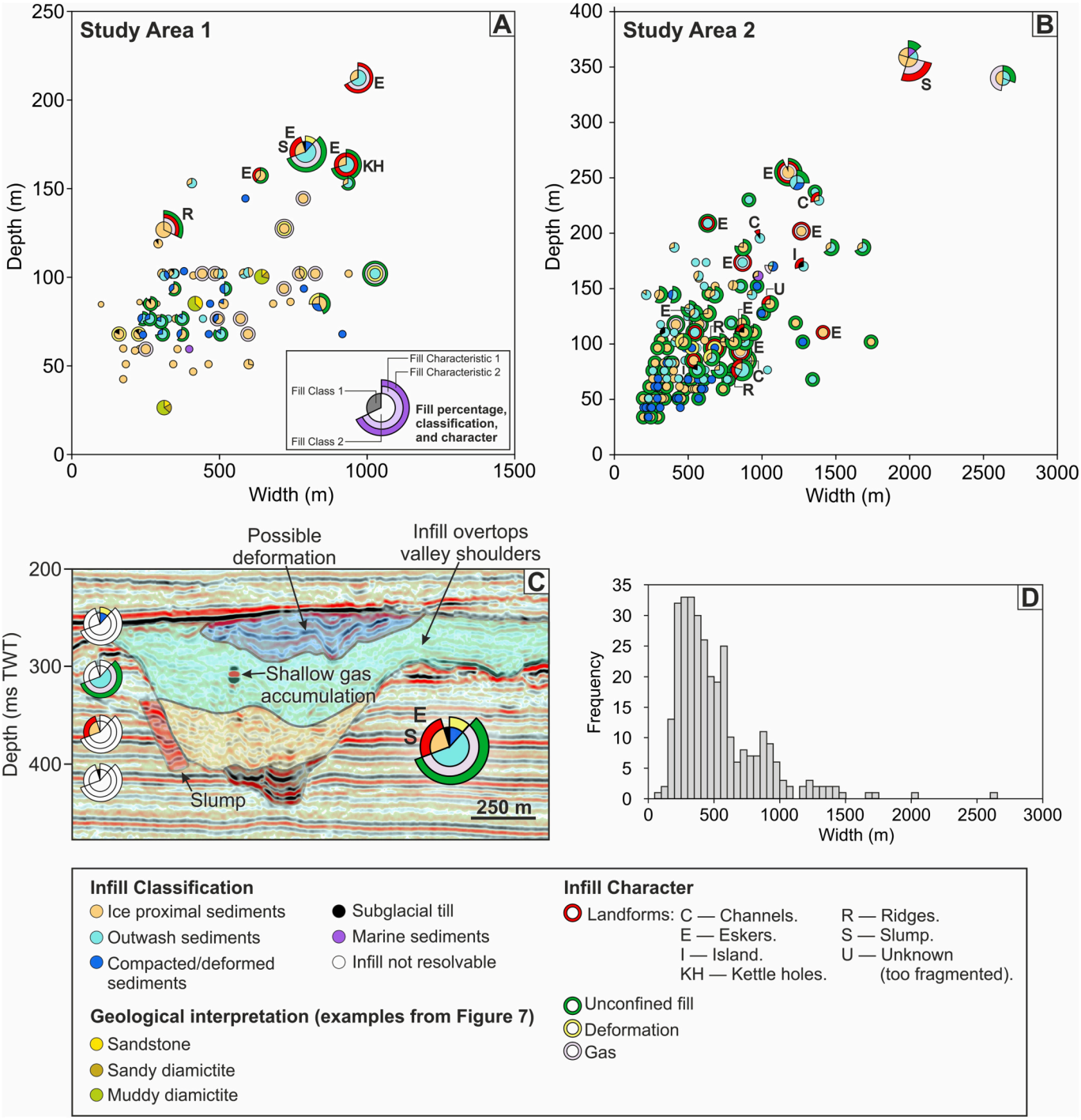

Fig. 8. Dimensions and infill character of tunnel valleys in the central North Sea. Inner pie charts display the percentage of each tunnel valley comprised of different fill units, coloured by infill classification. Outer rings surrounding specific pie chart segments indicate the character of the infill of that segment, such as whether the tunnel valley infill is deformed or contains evidence of landforms within it. Fill type is plotted in an anti-clockwise direction from base of the tunnel valley to its upper fill unit. Larger markers represent more complex infill architecture. (A) Dimensions and infill character of tunnel valleys in Study Area 1, and three examples of Late Ordovician tunnel valleys in North Africa (see Fig. 7 for context). (B) Dimensions and infill character of tunnel valleys in Study Area 2. (C) Example tunnel valley cross-section classified into different infill facies and containing characteristics such as slumps, eskers and shallow gas accumulations. (D) Histogram of tunnel valley widths from both study areas. Note that the figure scales are not consistent between (A) and (B).

Of the four other minor units contained within the central North Sea tunnel valleys, the imbricated reflections comprising Infill Unit 4 are interpreted as glaciotectonic thrust structures indicating sediment deformation by ice motion, based on comparison to similar features elsewhere (e.g., Huuse and Lykke-Andersen, 2000a). We interpret Infill Type 5 as marine sediments deposited near the top of the tunnel valleys, and Infill Type 6 as slump and mass-movement deposits present within the valleys (Kirkham et al., 2021; Kirkham et al., 2022). Finally, we interpret the reflections characterising Infill Type 7 as the top of discontinuous deposits of subglacial till plastered onto the floors of the tunnel valleys (Ó Cofaigh, 1996).

5.2. Patterns of tunnel valley sedimentation

Our systematic regional mapping of tunnel valley infill demonstrates that most tunnel valleys are characterised by a relatively simple fill architecture consisting of 1–2 seismic facies, although notably more complex examples of tunnel valley fill exist (up to 5 seismic facies); these are especially recognised in areas of HR3D seismic data coverage. The more complex infill patterns visible in the HR3D seismic data are more similar to the numerous sedimentary units described in borehole investigations (e.g., Hepp et al., 2012; up to 6 lithological units) than the more simple bi- or tripartite patterns previously interpreted from conventional 3D seismic data (e.g., Huuse and Lykke-Andersen, 2000b; Kluiving et al., 2003; Lonergan et al., 2006; Stewart et al., 2012). This shows that HR3D seismic data are capable of capturing fine-scale infill packages not visible in conventional 3D seismic data. Consequently, although the CNS MegaSurveyPlus used for the majority of the tunnel valley infill mapping in this study is higher resolution than previous compilations, the finer detail of tunnel valley fills is probably not fully resolved in the regions where HR3D seismic data coverage is absent. Furthermore, this issue is spatially variable because the presence of seismic multiples in some areas and other quality control issues (e.g., poor muting and velocity controls) can make it difficult to interpret the near-seabed interval of the 3D seismic data. Therefore, whilst conventional 3D seismic data are sufficient to map and classify the broad-scale structure of tunnel valley infill facies, HR3D seismic data is needed to reveal the true morphology and infill structures present within buried tunnel valleys.

Tunnel valleys with larger dimensions tend to contain greater numbers of fill units, a trend that is particularly apparent for the more recent generations (Fig. 8). At a gross scale, many tunnel valleys contain a previously reported deglacial succession of ice-proximal sediments overlain by distal outwash deposits that may overtop the valley shoulders (e.g., Cameron et al., 1987; Huuse and Lykke-Andersen, 2000b; Kluiving et al., 2003; Stewart et al., 2012; van der Vegt et al., 2012). Marine sediments are also present at the top of the largest valleys that were not fully infilled during deglaciation. This pattern of decreasing glacial influence reflects the retreat of the ice sheet front away from the tunnel valleys after these features were incised (Praeg, 1996; Ghienne and Deynoux, 1998; Janszen et al., 2012b; van der Vegt et al., 2012).

In contrast to previous studies, however, our detailed mapping using higher resolution 3D seismic data allows for a number of additional patterns to be drawn out. Previous investigations of tunnel valley infill in the North Sea have not been able to distinguish differences in the infill patterns of different tunnel valley generations (e.g., Stewart et al., 2012). Our updated mapping suggests that earlier tunnel valley generations (1–3) are characterised by simpler infill architectures than later tunnel valley generations. These earlier tunnel valley fills consist largely of ice-proximal sediments that sometimes contain evidence of ice overriding. We interpret these infill sequences to reflect sedimentation during relatively gradual ice-sheet retreat with occasional episodes of overriding by re-advancing grounded ice. Later generations of tunnel valleys (4–10) have more variable sedimentation patterns with a higher incidence of outwash sediments. Many examples of subglacial landforms, deformation structures, and shallow gas deposits are present within these later tunnel valley generations, potentially indicating more dynamic fluctuations of the ice margin (including readvances and stagnation) during valley filling and ice retreat.

In addition, extensive proglacial outwash sediments are particularly common further south in Study Area 2. This infill unit overtops the valley shoulders in over 50% of the tunnel valleys that contain it — a characteristic that appears to be independent of valley size. The reduced presence of ice-proximal sediments and the deposition of a regionally extensive blanket of unconfined outwash sediments in this region indicates that ice-margin retreat rates in this area were comparatively rapid — a pattern that occurred over multiple glaciations. The thickness and patterns of tunnel valley infill may also be indicative of relative retreat rates and the frequency of readvances of the ice margin in the geological record (Janszen et al., 2012b). For example, infill sequences in which distal outwash deposits are overlain by sediments deposited in an ice-proximal setting indicates a substantial readvance of the ice margin following initial ice retreat. In both of our study areas, incidences of this pattern are rare (<2%), indicating that substantial readvances of the ice margin followed by a more gradual retreat did not frequently occur during the deglaciation of the North Sea at times when the tunnel valleys were unfilled. However, a greater number of tunnel valleys in Study Area 2 (14%) are entirely filled with outwash sediments compared to those in Study Area 1 (3%), a trend that is particularly apparent for more recent tunnel valley generations (8–10). This pattern may indicate that the southern North Sea experienced greater ice marginal retreat rates compared to the central North Sea where thicker deposits of ice-proximal facies are present. These inferences are supported by numerical model and geomorphological reconstructions of the deglaciation of the North Sea during the last glacial period (Clark et al., 2022), which demonstrate that the unzipping of the British-Irish and Scandinavian ice sheets was rapid and was primarily driven by the retreat of the Norwegian Channel Ice Stream (Gandy et al., 2021).

An exception to this pattern is where landforms, in particular crevasse-squeeze ridges, are observed within the valley fills (Figs. 8, 9). Where observed, crevasse-squeeze ridges are buried within the outwash unit. Formatively linked to glacial surging (Sharp, 1985; Solheim and Pfirman, 1985), an absence of ice-proximal sediments above and below these ridges demonstrates that a rapid readvance and retreat of the ice margin occurred before and after ridge deposition, respectively. This suggests that in rare cases, rapid and substantial fluctuations (surges or readvances and stagnation) of the ice margin occurred during deglaciation, potentially facilitated by changing basal hydrological conditions within the tunnel valleys themselves (Kirkham et al., 2021). Other subglacial landforms buried within the tunnel valleys likely reflect minor seasonal readvances of the ice margin. For example, the formation of continuous and often laterally extensive (>14 km) depositional landforms such as eskers (Figs. 9, 10), rather than more discontinuous beaded structures, demonstrates that sediment supply outpaced ice retreat in these environments (Livingstone et al., 2020).

Landforms are most commonly present within larger tunnel valleys (wider than ~400 m and deeper than ~75 m), particularly within the deepest ones, and typically occur within valleys characterised by more complex infill patterns (>2 seismic facies) (Fig. 8). The glacitectonic mega-rafts interpreted within the infill of some valleys strongly resemble the rafts of substratum material sometimes contained within the basal fill of tunnel valleys in northwest Germany (Janszen et al., 2012a). These authors note that the rafts are primarily present downstream of valley-floor overdeepenings, potentially indicating the rapid headward valley erosion proposed for other Pleistocene tunnel valleys (Wingfield, 1990; Praeg, 1996; Hooke and Jennings, 2006; Janszen et al., 2012a). High-amplitude, phase-reversed seismic reflections and blanking of reflections associated with the presence of shallow gas (Fader, 1997) also occur most frequently within larger tunnel valleys with complex infill architectures. However, in contrast to the landforms which are present in most tunnel valley generations, shallow gas accumulations generally occur within older tunnel valley generations

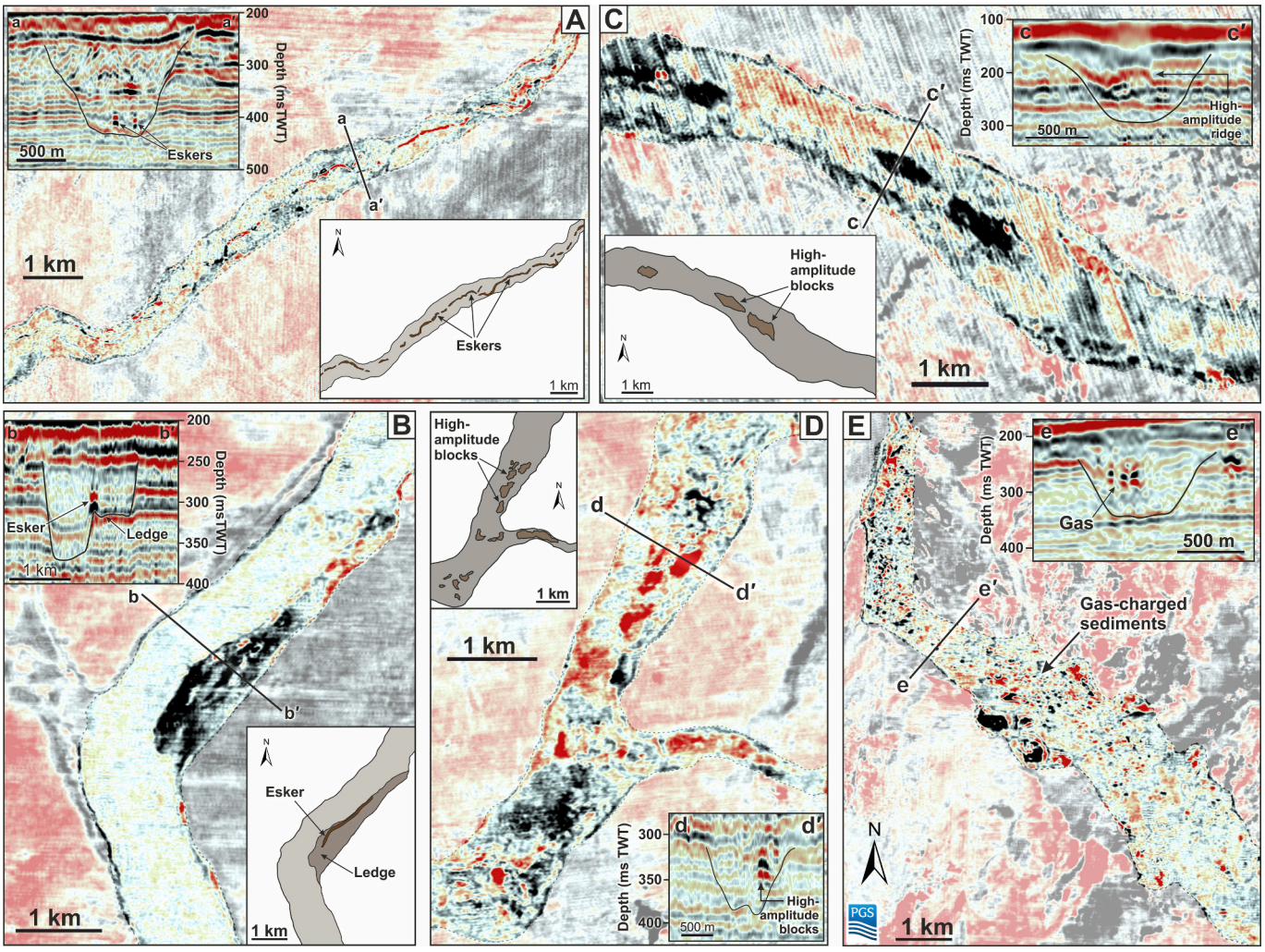

Fig. 9. High-amplitude reflections associated with subglacial landforms and shallow gas buried within the central North Sea tunnel valleys. (A, B) Examples of eskers and streamlined island-like blocks (C, D) buried within the infill of tunnel valleys. (E) Example of gas-charged tunnel valley infill sediments. All examples are from Study Area 2, however similar examples are also present in Study Area 1.

(Figs. 3D, 4D, S2, S3); this observation might indicate that the shallower sediments covering these tunnel valleys might be ineffective as a trap for gas in the younger valley generations.

The relative position of the subglacial landforms within the sedimentary facies that buries them within the tunnel valleys is capable of indicating relative retreat rates. Approximately 46% of the buried eskers observed in the tunnel valleys are situated between two layers of ice-proximal sediments. This pattern indicates that a readvance occurred over the first ice-proximal unit. The esker was then formed before the ice gradually retreated from the tunnel valley, depositing the second ice-proximal unit. The preservation of eskers also implies that there was little or no ice flow in the tunnel valley after the eskers formed; this situation could occur if ice margin had surged along the tunnel valley and then stagnated prior to esker formation (Kirkham et al., 2021). In contrast, a pattern of rapid ice-margin retreat following esker deposition is slightly more commonly observed as 54% of buried eskers are located at the boundary between ice-proximal and outwash sediments. This pattern indicates that a readvance of the ice margin, followed by esker deposition and then rapid lift off and retreat of the ice front occurred in these settings. The rapid retreat style implied by the presence of thick outwash sediments at the top of the tunnel valleys is supported by the association between this sedimentary facies and the higher continuity of eskers buried by this package compared to those buried by further ice-proximal sediments. This implies that the eskers were exposed from beneath a grounded ice sheet only briefly before being blanketed by outwash sediments, facilitating their excellent preservation compared to the slower ice retreat implied by the presence of ice-proximal sediments covering these features (Storrar et al., 2014; Storrar et al., 2019).

Eskers buried within the tunnel valleys are characterised by high-amplitude seismic reflections with phase-reversed polarity over the ridge crests (Figs. 9A–C, 10). Combined with acoustic masking of underlying reflectors, these characteristics suggest that the eskers often contain shallow gas within their constituent sediments (Fader, 1997; Buckley, 2012; Rose et al., 2018). Accordingly, when HR3D seismic data is available to use as a guide, it is possible to image eskers using conventional 3D seismic data as the shallow gas contained within them helps to illuminate them from the surrounding valley infill (Fig. 10D).

Correlation analysis between the eskers and the gas-charged Crenulate Reflector beneath them (Fyfe et al., 2003; Stoker et al., 2011) in one HR3D seismic dataset reveals little correlation between the location of gas accumulations within these features and their source rocks beneath (Fig. 11). This lack of correlation may indicate that the shallow gas contained within the eskers is biogenic in origin. However, in a different HR3D seismic dataset, the gas accumulations within one tunnel valley have clearly migrated along faults caused by salt diapirism (Fig. 12); similar occurrences of gas escape along faults related to salt structures have also been reported in other parts of the North Sea (Kuhlmann and Wong, 2008). As the coarse-grained deposits comprising

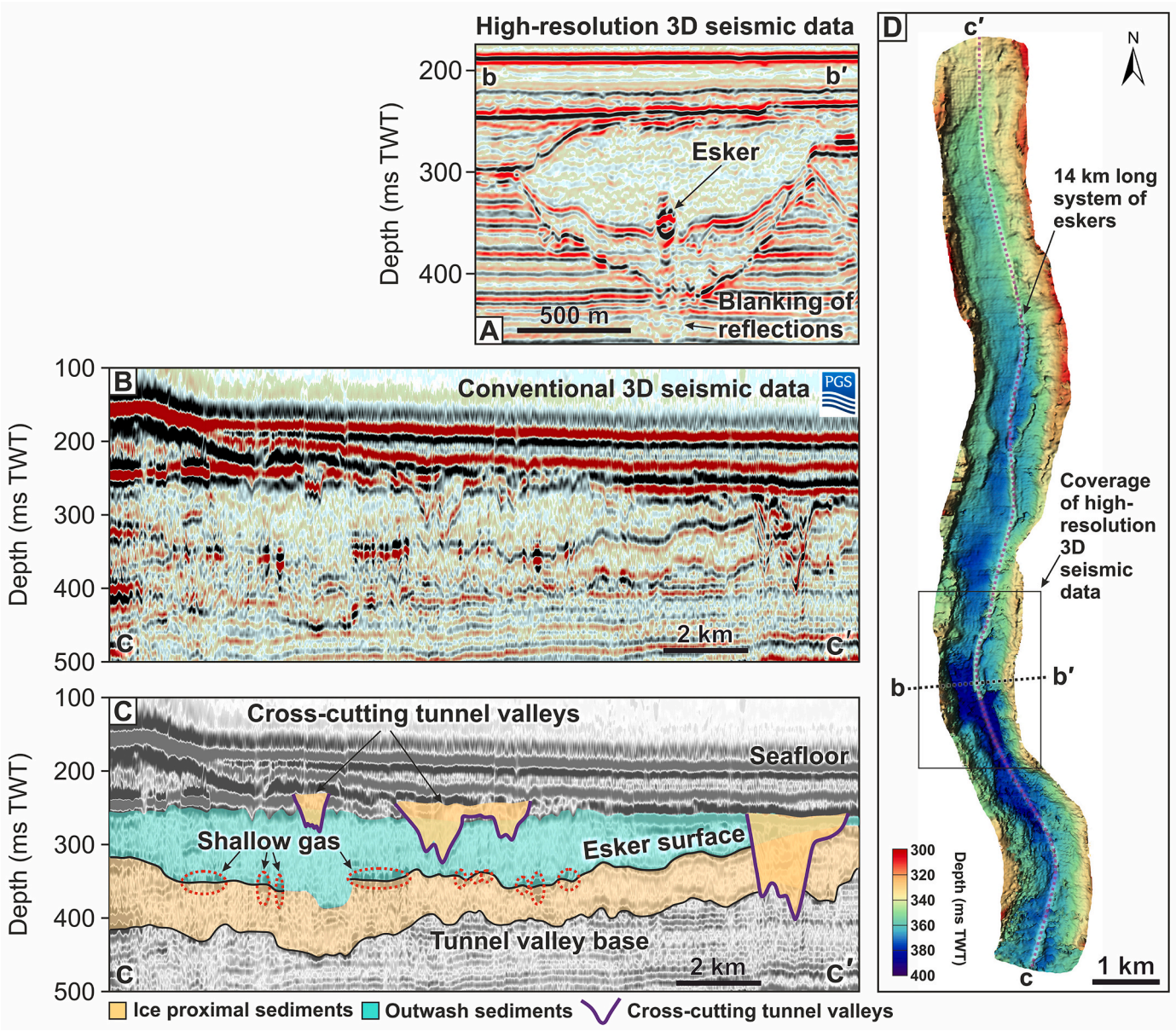

Fig. 10. Gas-charged eskers buried within tunnel valleys. (A) Cross-section of a tunnel valley in high-resolution 3D seismic data containing an esker characterised by a high-amplitude seismic reflection with phase-reversed polarity over the ridge crest. (B) Seismic profile along the length of the esker using conventional 3D seismic data, interpreted in (C). Stippled red lines indicate the locations of shallow gas anomalies. (D) Mapped seismic horizon in the centre of the tunnel valley infill corresponding to the esker reflection in conventional 3D seismic data. A 14-km long system of eskers can be visualised. (For interpretation of the references to colour in this figure legend, the reader is referred to the web version of this article.)

the eskers and other landforms commonly found within the infill of North Sea tunnel valleys represent high permeability pathways, fluids from the underlying strata would only need to migrate upwards into the tunnel valleys at a single point before they could migrate along these landforms to accumulate at local stratigraphic traps or even escape through the seafloor (Figs. 11B, 12C). Such near-surface accumulations within or at the intersection of tunnel valley walls (e.g., Fig. 11B) can create significant velocity contrasts with the surrounding strata, giving an impression of pipes or chimneys (Fig. 12B) below that may affect assessments of containment risk when scoping possible sites for carbon capture and storage or radioactive waste disposal (Karstens and Berndt, 2015; Frahm et al., 2020; Callow et al., 2021).

The extensive length (>14 km) and continuity of the gas-filled North Sea eskers demonstrates the significant geohazard that such structures potentially pose to the installation of near-seafloor infrastructure. Moreover, the ability for fluids to escape into tunnel valleys through faults, particularly in regions where salt domes are common, represents a significant mechanism to consider when detecting and monitoring CO_2 leakage from underlying carbon storage efforts (Raza et al., 2019) or even radioactive nuclear waste disposal (von Berlepsch and Haverkamp, 2016); if fluids were ever to migrate from storage reservoirs to the shallower depths in which these features are found, they would provide preferential pathways through which trapped gases could migrate laterally through or even escape from the subsurface.

Our inventory of tunnel valley infill supports the conclusions of previous studies which do not observe clinoform structures within valleys present in the central North Sea (Stewart et al., 2012). However, in the southern North Sea, tunnel valleys are filled with hundreds of metre-high, kilometre-long, clinoforms that dip northward towards the former ice-sheet centre(s) with angles of 0.5–12° (Laban, 1995; Praeg, 2003; Kristensen et al., 2007; Kristensen et al., 2008). These clinoform structures thus appear to be relatively unique to tunnel valleys present in the

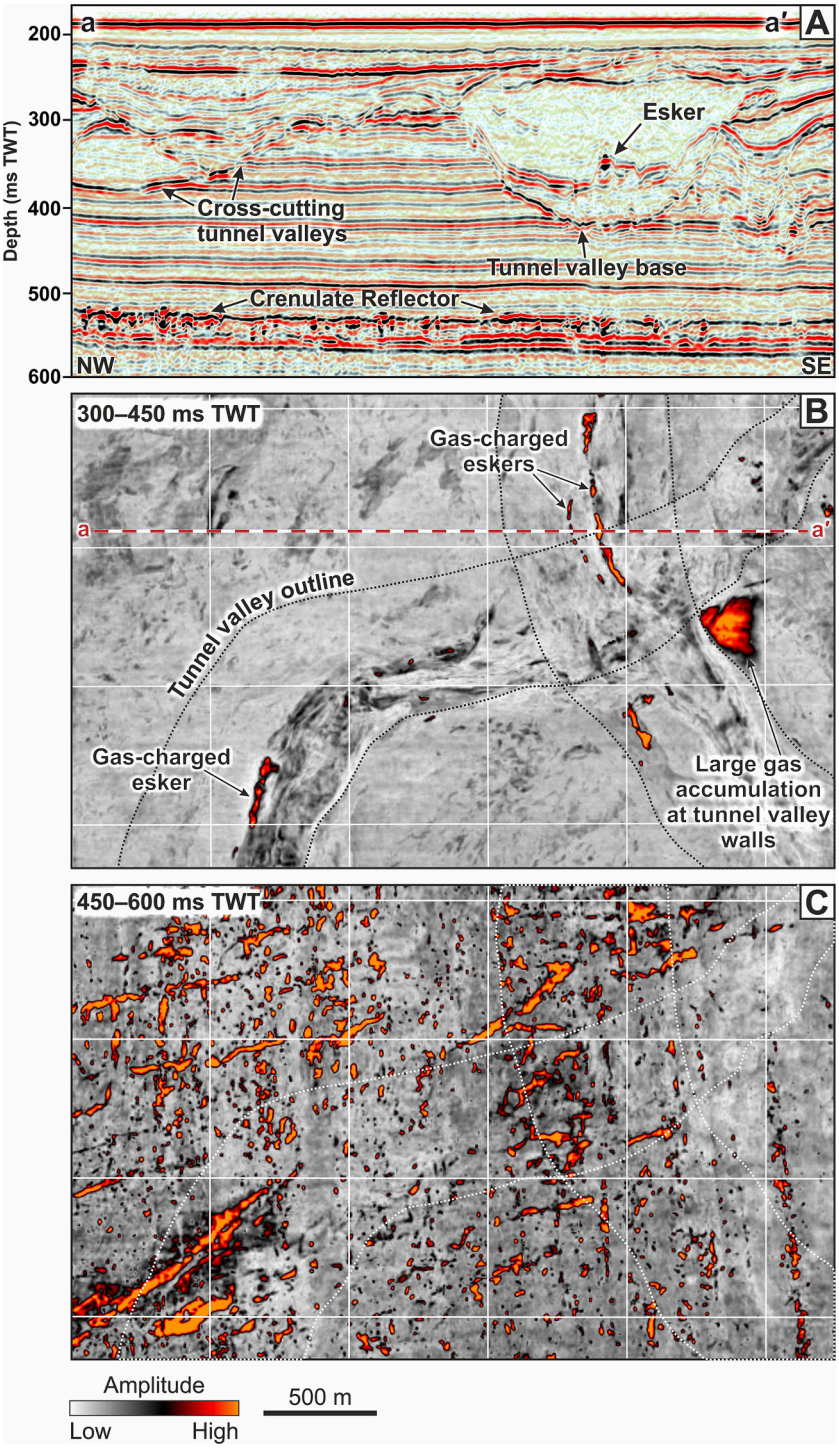

Fig. 11. Comparison of amplitude anomaly extractions between depths where tunnel valleys are present and the underlying gas-charged Crenulate Reflector. (A) High-resolution 3D seismic section of an esker buried within a tunnel valley, underlain by the Crenulate Reflector. (B) Plan-view RMS amplitude anomaly extraction at 300–450 ms TWT highlighting the locations of gas-charged eskers (high amplitudes). (C) Plan-view RMS amplitude anomaly extraction at 450–600 ms TWT displaying the gas-charged Crenulate Reflector. Stippled white lines delineate the tunnel valley boundaries. Solid white lines display the orientation of in-line and cross-line profiles.

southern North Sea, as they have not been confidently observed in outcrops onshore in northwest Europe (Ehlers et al., 1984; Benvenuti et al., 2018), although clinoform-like geometries have been recognised in outcrops of late Ordovician tunnel valleys preserved in north Africa (Le Heron et al., 2004). An exception to this trend is one tunnel valley covered by HR3D seismic data in the central northern North Sea (Study Area 3). Here, subtle structures resembling clinoforms are imaged from some orientations along the tunnel valley (Fig. S4A). The reflections have dip angles <4°, which is within the range of slopes reported from the well-known clinoform examples in the southern North Sea (1–11°), and dip towards the former ice-sheet centre in a similar manner to those filling the tunnel valleys present in the southern North Sea (Praeg, 1996; Kluiving et al., 2003; Kristensen et al., 2008). However, without further HR3D seismic data coverage, it is difficult to assess the scale and

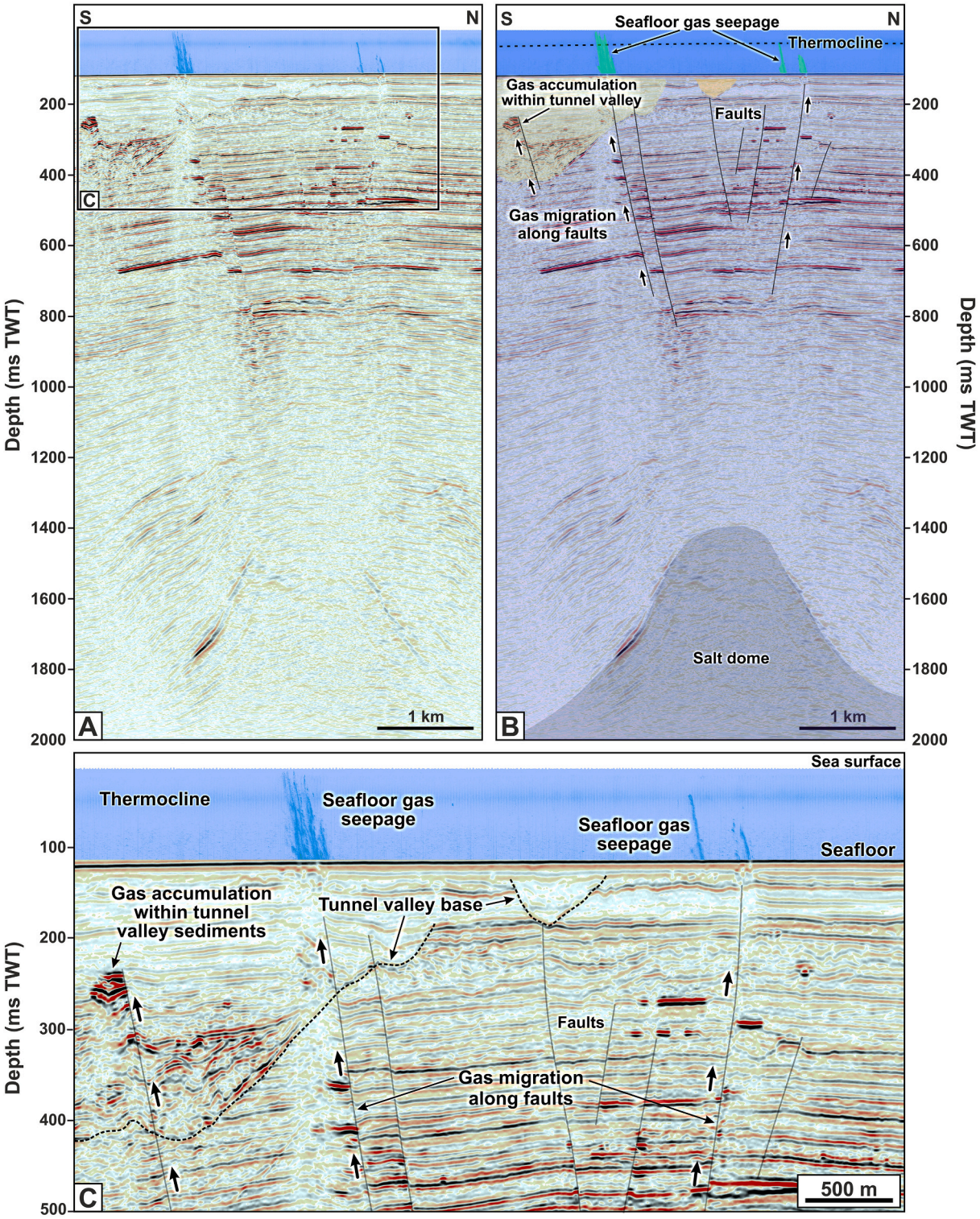

Fig. 12. Fluid migration into tunnel valleys along faults caused by salt diapirism. (A) High-resolution 3D seismic section with overlying water column backscatter data and (B) interpretation of a salt dome and overlying stratigraphy in the central southern North Sea. Salt diapirism has mobilised faults in the overlaying strata through which gas is seen to migrate; this gas eventually accumulates in (C) the tunnel valleys in uppermost part of the 3D seismic section, or escapes through the seafloor to form seeps which can be imaged in the water column backscatter data.

prevalence of these features within neighbouring valleys as they are difficult to detect using conventional 3D seismic data alone (Fig. S4C).

Another unusual feature of the tunnel valleys in Study Area 3 is the differential erosion of some filled tunnel valleys, leading to a domed profile (Fig. 5A, C, E). Streamlined glacial landforms located adjacent to the tunnel valleys demonstrate that they have been overridden by fast-flowing ice subsequent to their infilling with dense sands (e.g., Clark, 1993; Graham et al., 2007; King et al., 2009) (Fig. 5D). The dimensions, elongation ratios, and orientation of these landforms suggests that this region was overridden by a tributary of the Norwegian Channel Ice Stream. This fast-ice flow preferentially eroded the softer clay-dominated sediments surrounding the infilled valley, leaving the more

resistant tunnel valley infill standing proud of its surroundings (Fig. 5E). However, even the densely consolidated sands filling the tunnel valleys should have been relatively easy to erode by a grounded ice stream. Consequently, an additional factor potentially facilitated the unusual resistance of this material to glacial erosion, such as freezing or the accumulation of gas-hydrates.

Accumulations of subglacial gas-hydrates have been associated with areas of high basal traction — sticky spots — beneath palaeo ice streams in the Barents Sea (e.g., Winsborrow et al., 2016; Serov et al., 2017). The presence of gas hydrates can lead to an eight-fold increase in sediment shear strength through desiccating and stiffening their host sediments (e.g., Winters et al., 2004; Waite et al., 2009); this increase in sediment stiffness could have protected the tunnel valley sediments from the erosion of overriding ice. However, whilst there is some evidence for gas migration and escape through the tunnel valley sediments in the form of seabed pockmarks, phase-reversed reflections, and the blanking of underlying reflections, these indicators are not widespread in the locality of the tunnel valleys. Furthermore, any pockmarks that are present are not preferentially clustered above the tunnel valley fills as would be expected in the case of extensive gas hydrates being released in this area.

Alternatively, the sediments could have been strengthened through the incorporation of frozen water within them. The clinoforms noted within the southern North Sea tunnel valleys have been used as a basis to propose a 'backfilling' model of tunnel valley infilling close to the margin of a retreating ice sheet (Praeg, 2003; Kristensen et al., 2008). This theory postulates that tunnel valleys form and fill as a 'conveyor-belt' system, with sediment-laden meltwater produced in the ice-sheet interior being transported and plastered onto steep adverse bed slopes near the ice-sheet margin to form the clinoform structures through the process of glaciohydraulic supercooling. As the water becomes supercooled, thick sections of sediment-laden frazil and platy ice accrete onto the substratum sediments, trapping sediments in the ice (Alley et al., 1998; Lawson et al., 1998). Once deposited, the tunnel valley sediments could remain frozen due to the migration of groundwater from upstream regions, characterised by thicker ice and thus high pressures, towards the thinner ice marginal regions where it may freeze as it enters this lower pressure setting. The importance of tunnel valleys as groundwater reservoirs in many formerly glaciated settings supports this hypothesis (Sharpe et al., 1996; Piotrowski, 1997; BurVal Working Group, 2006; van der Vegt et al., 2012). Whilst many tunnel valleys mapped in this study contain a sandy facies that overtops the valley shoulders, it is notable that the tunnel valleys containing a domed proud-standing infill are also the only ones that contain subtle structures resembling clinoforms within them. If the clinoform-like structures interpreted within the tunnel valley are not artefacts, they could suggest that the freezing of water within these sediments, both during and after deposition, helped to protect these dome-shaped tunnel valley fills from subsequent ice-sheet overriding.

5.3. Implications for North Sea glacial history

Our revised classification of ten generations of tunnel valleys in the central North Sea is more complex than noted in previous investigations which have identified up to five generations of tunnel valleys in the eastern North Sea (Kristensen et al., 2007) and up to seven generations in the central North Sea (Stewart and Lonergan, 2011; Stewart et al., 2013; Ottesen et al., 2020). Indeed, the ten generations of tunnel valleys distinguished in the central North Sea makes this region the most complex pattern of tunnel valleys documented anywhere in the world. This difference derives from the higher-resolution data used to map buried tunnel valleys in this study. Although tunnel valleys in other regions such as Canada (Atkinson et al., 2013), mainland Europe (Jørgensen and Sandersen, 2006; Sandersen et al., 2009), the Barents Sea (Montelli et al., 2020), and North Africa (Douillet et al., 2012) commonly consist of multiple cross-cutting generations (van der Vegt et al., 2012), the number of generations observed rarely exceeds three — demonstrating the exceptional complexity of the tunnel valleys buried in the North Sea Basin. In some regions such as terrestrial Denmark, cut-and-fill structures within the infill of some tunnel valleys demonstrate that they have been reoccupied after being initially incised and partially filled, rather than forming a new generation (Jørgensen and Sandersen, 2006). In contrast, where resolvable, tunnel valleys in the central North Sea can contain smaller braided channel structures along their erosional base which likely migrated laterally as the valleys were incised (Kirkham et al., 2021; Kirkham et al., 2022). However, to date, no smaller channel structures have been resolved within the infill of the valleys themselves.

We speculate that the far greater number of tunnel valley generations present in the North Sea potentially reflects the extremely flat topography of the North Sea Basin due to the reduced influence of basal topography on determining the dominant direction of subglacial water routing. Although the routing of water beneath ice masses is controlled primarily by the ice surface profile (Shreve, 1972), basal topography still provides some constraint, especially if the basal topography is rugged. The exceptionally flat nature of the infilled North Sea Basin means that water routing in the region would have been highly sensitive to changes in ice sheet geometries (Kirkham et al., 2022); subtle changes in ice sheet profile created as the ice sheets covering the North Sea waxed and waned would therefore have significantly altered basal hydrological potential gradients, and thus subglacial water routing, over relatively short timescales. These prominent switches in water flow direction would tend to incise new generations of cross-cutting tunnel valleys rather than reoccupy existing features. In contrast, the more rugged subglacial topography of regions such as inland Britain, Western Europe or Scandinavia would have funnelled the routing of subglacial water into more persistent or similar flow pathways, resulting in the preferential reuse of existing older valleys rather than the incision of cross-cutting new tunnel valley generations.

The presence of even more generations of cross-cutting tunnel valley networks in the central North Sea adds weight to the growing body of evidence that the traditional model of northwest Europe's glacial history is too simplistic (See Section 3) and likely consists of more than three major glaciations over the last 460 kyr (Ehlers et al., 1984; Ehlers and Gibbard, 2007; Stewart and Lonergan, 2011; Lang et al., 2018; Batchelor et al., 2019; Ottesen et al., 2020; Lohrberg et al., 2022). Accurately constraining the age of tunnel valleys in the North Sea is notoriously difficult due to a lack of datable fossils and a general paucity of boreholes from within tunnel valleys. Evidence for grounded ice in the North Sea extends back to 1.87 Ma (Rea et al., 2018), potentially providing a large range of time in which the tunnel valleys could have first been incised. Palaeomagnetic evidence from British Geological Survey borehole 77/03 (Stoker et al., 1983) allowed Stewart and Lonergan (2011) to infer that the oldest of their tunnel valley generations mapped in the central North Sea was younger than the Brunhes-Matuyama magnetic reversal event at 780 ka. As six formally named cold marine isotope stages are observed in the ocean record over this period (Cohen and Gibbard, 2019), Stewart and Lonergan (2011) then correlated each of their seven generations of tunnel valleys to an individual cold stage present in the marine isotope record, with the oldest being of Elsterian age (MIS 12). The third and fourth tunnel valley generations were thought to represent reoccupation of valleys due to local advances and retreats of the ice margin as part of a larger glaciation (MIS 10 or 8). Evidence for valley reoccupation between and during subsequent glaciations has also been found in both onshore and offshore records (e.g., Müther et al., 2012; Roskosch et al., 2015).

The additional tunnel valley generations revealed by our revised mappings complicate this simple correlation. We offer two possible explanations for the additional tunnel valley generations identified in this study. First, the additional buried generations may represent additional tunnel valley forming glaciations in the central North Sea that extend further back than the Elsterian (MIS 12), as has been suggested for the southeastern North Sea (Lohrberg et al., 2022). Further cold periods,

younger than the Brunhes-Matuyama magnetic reversal event and older than the Elsterian, in which tunnel valleys could have potentially formed occurred in MIS 14, 16, and 18.

An alternative interpretation for the additional tunnel valley generations is that further tunnel valley generations were formed, filled, and re-incised relatively quickly as part of minor retreats and readvances during a larger glacial episode i.e., more than one generation of tunnel valley formed per glaciation. Although rare, coupled lithological and biostratigraphical data (Sandersen et al., 2009; Giglio et al., 2021), as well as numerical modelling experiments (Kirkham et al., 2022) suggest that tunnel valleys can form in just a few hundred to a few thousand years during deglaciation. Thus, if sedimentation rates were sufficiently high to infill the tunnel valleys rapidly after they formed, especially with sediments that are resistant to further glacial erosion such as the very dense sands observed in Study Area 3, it would potentially be possible to incise a new generation of cross-cutting tunnel valleys during minor fluctuations of the ice sheet configuration within a longer glacial period. Episodes of abrupt climate change — Dansgaard–Oeschger events — have been identified in ice-core records from Greenland (Bond et al., 1993; Dansgaard et al., 1993; Andersen et al., 2004), in which temperatures increased rapidly by 10–15 °C from cold stadial to warmer interstadial conditions within a few decades (Severinghaus and Brook, 1999; Huber et al., 2006; Kindler et al., 2014). These interstadial states typically lasted for 500–2000 years before gradually cooling — similar to the timescales required to erode tunnel valleys beneath ice sheets experiencing significant surface melting (Kirkham et al., 2022). As the direction of subglacial water drainage on flat and homogeneous ice sheet beds is controlled by the surface topography of ice sheets (Shreve, 1972), we speculate that subtle reconfigurations of ice-sheet topography during ice-sheet readvances following a Dansgaard–Oeschger event could produce consecutive generations of tunnel valleys with different orientations and locations within a single glacial period (Lelandais et al., 2018).

If this latter interpretation is correct, it is interesting to note that although the North Sea has been glaciated by grounded ice sheets for up to 1.87 million years, the majority of tunnel valleys appear to have been formed within the last ~500,000 years (Stewart and Lonergan, 2011; Lee et al., 2012; Ottesen et al., 2020). This could indicate that the dominant driver of ice-sheet retreat in this setting switched to a meltwater intensive retreat style around 500,000 years ago, leading to the formation of large networks of tunnel valleys in subsequent glaciations. Ice core records from Antarctica demonstrate that there was less pronounced warmth in interglacial periods prior to 430,000 years ago (Augustin et al., 2004). Interglacials after the Mid-Bruhnes Transition at ~430,000 years ago experienced warmer temperatures, higher concentrations of atmospheric CO_2, and an increase in the amplitude of the 100 kyr climate cycles compared to earlier interglacial periods (Augustin et al., 2004; Jouzel et al., 2007; Lüthi et al., 2008). Recent statistical analysis demonstrates that the Mid-Bruhnes Transition was a globally synchronous phenomenon that included other components of the climate system (Barth et al., 2018). The increased amplitude of glacial terminations following the Mid-Bruhnes Transition may thus have resulted in a more meltwater intensive regime than in previous glacial terminations; this climatic change could explain why abundant tunnel valleys began to form in the North Sea at around this time.

In either case, the greater number of tunnel valley generations presented in our revised mapping is consistent with previous analyses which postulate that tunnel valleys can form rapidly beneath ice sheets (Sandersen et al., 2009; Kirkham et al., 2022), and lends support to a more complex glacial history of northwest Europe than traditionally assumed. Further absolute dating constraints from boreholes and shallow drilling within tunnel valleys is ultimately required to better constrain their chronology, and therefore the glacial history of the North Sea, with greater accuracy.

6. Conclusions

Our study represents the most detailed attempt to characterise the infill of buried Quaternary tunnel valleys in the central North Sea to date. Improved regional 3D and state-of-the-art HR3D seismic data reveal ten cross-cutting generations of tunnel valleys buried beneath the seafloor of the central and central southern North Sea where only seven were visible previously. Our results support models of a more complex glacial history in western Europe than traditionally considered, and potentially suggest that it is possible to rapidly erode and infill multiple generations of tunnel valleys within a single glacial cycle. Further chronological constraints from boreholes are required to confirm or refute these hypotheses in the future.

Although the infill architecture of the tunnel valleys in the North Sea is immensely variable, advances in the resolution of 3D seismic data permit some subtle patterns to be drawn out which are unresolvable in previous datasets. The number of facies distinguishable in HR3D seismic data is similar to the number of sedimentary units described in borehole investigations; HR3D seismic data are therefore capable of revealing the true morphology and infill structures present within buried tunnel valleys. The overall pattern of tunnel valley infill in the North Sea records decreasing ice sheet influence towards the top of the tunnel valleys and reflects the retreat of the ice sheet margin away from the features after they are incised. At a more subtle level, earlier tunnel valley generations contain simpler infill architectures than later tunnel valley generations, reflecting sedimentation during relatively gradual ice-sheet retreat with occasional episodes of overriding by re-advancing grounded ice. Tunnel valleys formed in more recent glaciations have more variable sedimentation patterns with a higher incidence of outwash sediments, buried subglacial landforms, and deformation structures that potentially reflect more dynamic fluctuations of the ice margin (including readvances and stagnation) during valley filling and ice retreat in recent glaciations.

Delicate subglacial landforms such as eskers and crevasse-squeeze ridges are imaged within the tunnel valleys and imply that tunnel valley formation is linked to dynamic ice-sheet behaviour in areas where meltwater production rates are high. These landforms may contain shallow gas accumulations that represent a geohazard for seafloor infrastructure installation. In addition, we document instances where salt diapirism has caused fluids to migrate upwards through faults and into the near-surface tunnel valleys. In instances where this occurs, the relatively porous and often highly continuous subglacial landforms present within their infill may allow these fluids to spread laterally for kilometres or even escape from the seafloor; this process has implications for monitoring CO_2 leakage pathways from sub-surface carbon storage efforts in areas where tunnel valleys are present. Our results underline the importance of considering tunnel valleys as regulators of ice-sheet dynamics in models of future ice-sheet change, and the need to survey these features at high resolution when attempting to install infrastructure or undertake carbon capture and storage in formerly glaciated regions.

Author contributions

J.D.K., K.A.H., R.D.L., J.A.D., N.S.A. and M.H. conceived the study. E.S., K.G. and M.H. worked with data owners to gain permission for the use of the 3D seismic data in this project. J.D.K. analysed the 3D seismic data with contributions from K.A.H., R.D.L., J.A.D., E.S., M.H., M.A.S., D.O., D.P.L.H., A.L. and I.K. D.P.L.H. provided the Late Ordovician tunnel valley data. J.D.K. wrote the initial draft of the manuscript and produced the figures. All authors contributed to data interpretation and writing of the final paper.

Declaration of Competing Interest

The authors declare no competing interests.

Data availability

The confidential industry datasets analysed in this study are owned by bp, Harbour Energy, CNOOC, Equinor Energy AS, Petoro AS, Aker BP ASA, TotalEnergies EP Norge AS, TGS and PGS. Requests to access interpretations from these data should be referred to the lead author, or Ed Self at Gardline Ltd.

Acknowledgements

We thank bp, Harbour Energy, CNOOC, Equinor Energy AS, Petoro AS, Aker BP ASA, TotalEnergies EP Norge AS, TGS and PGS for access and permission to publish images extracted from the HR3D seismic data, UHR2D seismic data and the Central North Sea MegaSurveyPlus. S&P Global and Schlumberger are thanked for providing academic seismic interpretation software licenses. James D. Kirkham is supported by the Natural Environment Research Council (grant NE/L002507/1). Kelly A. Hogan and Robert D. Larter were supported by the Natural Environment Research Council – British Antarctic Survey Polar Science for Planet Earth programme. We thank Christian Huebscher and two anonymous reviewers for helpful comments that improved the manuscript. The interpretations made in this paper are the views of the authors and not necessarily those of the license owners.

Appendix A. Supplementary data

Supplementary data to this article can be found online at https://doi.org/10.1016/j.margeo.2023.107185.

References

Alley, R.B., Lawson, D.E., Evenson, E.B., Strasser, J.C., Larson, G.J., 1998. Glaciohydraulic supercooling: a freeze-on mechanism to create stratified, debris-rich basal ice: II. Theory. J. Glaciol. 44 (148), 563–569. https://doi.org/10.3189/S0022143000002070.

Andersen, K.K., Azuma, N., Barnola, J.M., Bigler, M., Biscaye, P., Caillon, N., Chappellaz, J., Clausen, H.B., Dahl-Jensen, D., Fischer, H., Flückiger, J., Fritzsche, D., Fujii, Y., Goto-Azuma, K., Grønvold, K., Gundestrup, N.S., Hansson, M., Huber, C., Hvidberg, C.S., Johnsen, S.J., Jonsell, U., Jouzel, J., Kipfstuhl, S., Landais, A., Leuenberger, M., Lorrain, R., Masson-Delmotte, V., Miller, H., Motoyama, H., Narita, H., Popp, T., Rasmussen, S.O., Raynaud, D., Rothlisberger, R., Ruth, U., Samyn, D., Schwander, J., Shoji, H., Siggard-Andersen, M.L., Steffensen, J. P., Stocker, T., Sveinbjörnsdóttir, A.E., Svensson, A., Takata, M., Tison, J.L., Thorsteinsson, T., Watanabe, O., Wilhelms, F., White, J.W.C., North Greenland Ice Core Project, m, 2004. High-resolution record of Northern Hemisphere climate extending into the last interglacial period. Nature 431 (7005), 147–151. https://doi.org/10.1038/nature02805.

Anell, I., Thybo, H., Rasmussen, E., 2012. A synthesis of Cenozoic sedimentation in the North Sea. Basin Res. 24 (2), 154–179. https://doi.org/10.1111/j.1365-2117.2011.00517.x.

Atkinson, N., Andriashek, L.D., Slattery, S.R., 2013. Morphological analysis and evolution of buried tunnel valleys in Northeast Alberta, Canada. Quat. Sci. Rev. 65, 53–72. https://doi.org/10.1016/j.quascirev.2012.11.031.

Augustin, L., Barbante, C., Barnes, P.R.F., Marc Barnola, J., Bigler, M., Castellano, E., Cattani, O., Chappellaz, J., Dahl-Jensen, D., Delmonte, B., Dreyfus, G., Durand, G., Falourd, S., Fischer, H., Flückiger, J., Hansson, M.E., Huybrechts, P., Jugie, G., Johnsen, S.J., Jouzel, J., Kaufmann, P., Kipfstuhl, J., Lambert, F., Lipenkov, V.Y., Littot, G.C., Longinelli, A., Lorrain, R., Maggi, V., Masson-Delmotte, V., Miller, H., Mulvaney, R., Oerlemans, J., Oerter, H., Orombelli, G., Parrenin, F., Peel, D.A., Petit, J.-R., Raynaud, D., Ritz, C., Ruth, U., Schwander, J., Siegenthaler, U., Souchez, R., Stauffer, B., Peder Steffensen, J., Stenni, B., Stocker, T.F., Tabacco, I.E., Udisti, R., van de Wal, R.S.W., van den Broeke, M., Weiss, J., Wilhelms, F., Winther, J.-G., Wolff, E.W., Zucchelli, M., members, E. c., and members, E. c, 2004. Eight glacial cycles from an Antarctic ice core. Nature 429 (6992), 623–628. https://doi.org/10.1038/nature02599.

Barth, A.M., Clark, P.U., Bill, N.S., He, F., Pisias, N.G., 2018. Climate evolution across the Mid-Brunhes transition. Clim. Past 14 (12), 2071–2087. https://doi.org/10.5194/cp-14-2071-2018.

Batchelor, C.L., Ottesen, D., Dowdeswell, J.A., 2017. Quaternary evolution of the northern North Sea margin through glacigenic debris-flow and contourite deposition. J. Quat. Sci. 32 (3), 416–426. https://doi.org/10.1002/jqs.2934.

Batchelor, C.L., Margold, M., Krapp, M., Murton, D.K., Dalton, A.S., Gibbard, P.L., Stokes, C.R., Murton, J.B., Manica, A., 2019. The configuration of Northern Hemisphere ice sheets through the Quaternary. Nat. Commun. 10 (1), 3713. https://doi.org/10.1038/s41467-019-11601-2.

Batchelor, C.L., Bellwald, B., Planke, S., Ottesen, D., Henriksen, S., Myklebust, R., Johansen, S.E., Dowdeswell, J.A., 2021. Glacial, fluvial and contour-current-derived sedimentation along the northern North Sea margin through the Quaternary. Earth Planet. Sci. Lett. 566, 116966 https://doi.org/10.1016/j.epsl.2021.116966.

Beaud, F., Flowers, G.E., Venditti, J.G., 2016. Efficacy of bedrock erosion by subglacial water flow. Earth Surf. Dyn. 4 (1), 125–145. https://doi.org/10.5194/esurf-4-125-2016.

Beaud, F., Venditti, J.G., Flowers, G.E., Koppes, M., 2018. Excavation of subglacial bedrock channels by seasonal meltwater flow. Earth Surf. Process. Landf. 43 (9), 1960–1972. https://doi.org/10.1002/esp.4367.

Benvenuti, A., Šegvić, B., Moscariello, A., 2018. Tunnel valley deposits from the southern North Sea - material provenance and depositional processes. Boreas 47 (2), 625–642. https://doi.org/10.1111/bor.12292.

Bond, G., Broecker, W., Johnsen, S., McManus, J., Labeyrie, L., Jouzel, J., Bonani, G., 1993. Correlations between climate records from North Atlantic sediments and Greenland ice. Nature 365 (6442), 143–147. https://doi.org/10.1038/365143a0.

Breuer, S., Bebiolka, A., Noack, V., Lang, J., 2023. The past is the key to the future – considering Pleistocene subglacial erosion for the minimum depth of a radioactive waste repository. E&G Q. Sci. J. 72 (1), 113–125. https://doi.org/10.5194/egqsj-72-113-2023.

Buckley, F.A., 2012. An Early Pleistocene grounded ice sheet in the Central North Sea. In: Huuse, M., Redfern, J., Le Heron, D.P., Dixon, R., Moscariello, A., Craig, J. (Eds.), Glaciogenic Reservoirs and Hydrocarbon Systems, vol. 368. Geological Society, London, Special Publications, pp. 185–209.

BurVal Working Group, 2006. Groundwater resources in buried valleys: a challenge for geosciences. GGA-Inst.

Callow, B., Bull, J.M., Provenzano, G., Böttner, C., Birinci, H., Robinson, A.H., Henstock, T.J., Minshull, T.A., Bayrakci, G., Lichtschlag, A., Roche, B., Yilo, N., Gehrmann, R., Karstens, J., Falcon-Suarez, I.H., Berndt, C., 2021. Seismic chimney characterisation in the North Sea – Implications for pockmark formation and shallow gas migration. Mar. Pet. Geol. 133, 105301 https://doi.org/10.1016/j.marpetgeo.2021.105301.

Cameron, T.D.J., Stoker, M.S., Long, D., 1987. The history of Quaternary sedimentation in the UK sector of the North Sea Basin. J. Geol. Soc. Lond. 144, 43–58. https://doi.org/10.1144/gsjgs.144.1.0043.

Clark, C.D., 1993. Mega-scale glacial lineations and cross-cutting ice-flow landforms. Earth Surf. Process. Landf. 18, 1–29. https://doi.org/10.1002/esp.3290180102.

Clark, C.D., Gibbard, P.L., Rose, J., 2004. Pleistocene glacial limits in England, Scotland and Wales. In: Ehlers, J., Gibbard, P.L. (Eds.), Developments in Quaternary Sciences, vol. 2. Elsevier, pp. 47–82.

Clark, P.U., Archer, D., Pollard, D., Blum, J.D., Rial, J.A., Brovkin, V., Mix, A.C., Pisias, N. G., Roy, M., 2006. The middle Pleistocene transition: characteristics, mechanisms, and implications for long-term changes in atmospheric pCO2. Quat. Sci. Rev. 25 (23), 3150–3184. https://doi.org/10.1016/j.quascirev.2006.07.008.

Clark, C.D., Ely, J.C., Greenwood, S.L., Hughes, A.L.C., Meehan, R., Barr, I.D., Bateman, M.D., Bradwell, T., Doole, J., Evans, D.J.A., Jordan, C.J., Monteys, X., Pellicer, X.M., Sheehy, M., 2018. BRITICE Glacial Map, version 2: a map and GIS database of glacial landforms of the last British-Irish Ice Sheet. Boreas 47 (1), 11–27. https://doi.org/10.1111/bor.12273.

Clark, C.D., Ely, J.C., Hindmarsh, R.C.A., Bradley, S., Ignéczi, A., Fabel, D., Ó Cofaigh, C., Chiverrell, R.C., Scourse, J., Benetti, S., Bradwell, T., Evans, D.J.A., Roberts, D.H., Burke, M., Callard, S.L., Medialdea, A., Saher, M., Small, D., Smedley, R.K., Gasson, E., Gregoire, L., Gandy, N., Hughes, A.L.C., Ballantyne, C., Bateman, M.D., Bigg, G.R., Doole, J., Dove, D., Duller, G.A.T., Jenkins, G.T.H., Livingstone, S.L., McCarron, S., Moreton, S., Pollard, D., Praeg, D., Sejrup, H.P., Van Landeghem, K.J. J., Wilson, P., 2022. Growth and retreat of the last British–Irish Ice Sheet, 31 000 to 15 000 years ago: the BRITICE-CHRONO reconstruction. Boreas. https://doi.org/10.1111/bor.12594.

Clerc, S., Buoncristiani, J.-F., Guiraud, M., Vennin, E., Desaubliaux, G., Portier, E., 2013. Subglacial to proglacial depositional environments in an Ordovician glacial tunnel valley, Alnif, Morocco. Palaeogeogr. Palaeoclimatol. Palaeoecol. 370, 127–144. https://doi.org/10.1016/j.palaeo.2012.12.002.

Cohen, K.M., Gibbard, P.L., 2019. Global chronostratigraphical correlation table for the last 2.7 million years, version 2019 QI-500. Quat. Int. 500, 20–31. https://doi.org/10.1016/j.quaint.2019.03.009.

Coughlan, M., Fleischer, M., Wheeler, A.J., Hepp, D.A., Hebbeln, D., Mörz, T., 2018. A revised stratigraphical framework for the Quaternary deposits of the German North Sea sector: a geological-geotechnical approach. Boreas 47 (1), 80–105. https://doi.org/10.1111/bor.12253.

Dahlgren, K.I.T., Vorren, T.O., Laberg, J.S., 2002. Late Quaternary glacial development of the mid-Norwegian margin—65 to 68°N. Mar. Pet. Geol. 19 (9), 1089–1113. https://doi.org/10.1016/S0264-8172(03)00004-7.

Dansgaard, W., Johnsen, S.J., Clausen, H.B., Dahl-Jensen, D., Gundestrup, N.S., Hammer, C.U., Hvidberg, C.S., Steffensen, J.P., Sveinbjörnsdottir, A.E., Jouzel, J., Bond, G., 1993. Evidence for general instability of past climate from a 250-kyr ice-core record. Nature 364 (6434), 218–220. https://doi.org/10.1038/364218a0.

Douillet, G., Ghienne, J.F., Géraud, Y., Abueladas, A., Diraison, M., Al-Zoubi, A., 2012. Late Ordovician tunnel valleys in southern Jordan. Geol. Soc. Lond. Spec. Publ. 368 (1), 275–292. https://doi.org/10.1144/sp368.4.

Dowdeswell, J.A., Ottesen, D., 2013. Buried iceberg ploughmarks in the early Quaternary sediments of the central North Sea: a two-million year record of glacial influence from 3D seismic data. Mar. Geol. 344, 1–9. https://doi.org/10.1016/j.margeo.2013.06.019.

Dowdeswell, J.A., Hogan, K.A., Arnold, N.S., Mugford, R.I., Wells, M., Hirst, J.P.P., Decalf, C., 2015. Sediment-rich meltwater plumes and ice-proximal fans at the margins of modern and ancient tidewater glaciers: observations and modelling. Sedimentology 62 (6), 1665–1692. https://doi.org/10.1111/sed.12198.

Ehlers, J., 1990. Reconstructing the dynamics of the north-west european Pleistocene ice sheets. Quat. Sci. Rev. 9, 71–83. https://doi.org/10.1016/0277-3791(90)90005-U.
Ehlers, J., Gibbard, P.L., 2007. The extent and chronology of Cenozoic Global Glaciation. Quat. Int. 164-165, 6–20. https://doi.org/10.1016/j.quaint.2006.10.008.
Ehlers, J., Linke, G., 1989. The origin of deep buried channels of Elsterian age in Northwest Germany. J. Quat. Sci. 4 (3), 255–265. https://doi.org/10.1002/jqs.3390040306.
Ehlers, J., Wingfield, R., 1991. The extension of the Late Weichselian/Late Devensian ice sheets in the North Sea Basin. J. Quat. Sci. 6 (4), 313–326. https://doi.org/10.1002/jqs.3390060406.
Ehlers, J., Meyer, K.D., Stephan, H.J., 1984. The pre-Weichselian glaciations of north-west Europe. Quat. Sci. Rev. 3 (1), 1–40. https://doi.org/10.1016/0277-3791(84)90003-9.
Eidvin, T., Rundberg, Y., 2001. Late Cainozoic stratigraphy of the Tampen area (Snorre and Visund fields) in the northern North Sea, with emphasis on the chronology of early Neogene sands. Nor. J. Geol. 81, 119–160.
Evans, D.J.A., Atkinson, N., Phillips, E., 2020. Glacial geomorphology of the Neutral Hills Uplands, Southeast Alberta, Canada: the process-form imprints of dynamic ice streams and surging ice lobes. Geomorphology 350, 106910. https://doi.org/10.1016/j.geomorph.2019.106910.
Fader, G.B.J., 1997. The effects of shallow gas on seismic reflection profiles. In: Davies, T. A., Bell, T., Cooper, A.K., Josenhans, H., Polyak, L., Solheim, A., Stoker, M.S., Stravers, J.A. (Eds.), Glaciated Continental Margins: An Atlas of Acoustic Images: Dordrecht. Springer, Netherlands, pp. 29–30.
Frahm, L., Hübscher, C., Warwel, A., Preine, J., Huster, H., 2020. Misinterpretation of velocity pull-ups caused by high-velocity infill of tunnel valleys in the southern Baltic Sea. Near Surf. Geophys. https://doi.org/10.1002/nsg.12122.
Fyfe, J., Gregersen, U., Jordt, H., Rundberg, Y., Eidvin, T., Evans, D., Stewart, D., Hovland, M., Andresen, P., 2003. Oligocene to holocene. In: The Millennium Atlas: Petroleum Geology of the Central and Northern North Sea, 279. Geological Society, London, p. 287.
Games, K.P., 2012. Shallow gas detection - why HRS, why 3D, why not HRS 3D? First Break 30, 25–33. https://doi.org/10.3997/1365-2397.2012016.
Games, K.P., Self, E., 2017. HRS 3D data — a fundamental change in site survey geohazard interpretation. First Break 35 (2152). https://doi.org/10.3997/1365-2397.2017008.
Games, K.P., Wakefield, N.D., 2014. The successful design, development and acquisition of a UHRS 3D seismic dataset. Near Surf. Geosci. Athens, Greece. https://doi.org/10.3997/2214-4609.20142132.
Gandy, N., Gregoire, L.J., Ely, J.C., Cornford, S.L., Clark, C.D., Hodgson, D.M., 2021. Collapse of the Last Eurasian Ice Sheet in the North Sea modulated by combined processes of ice flow, surface melt, and marine ice sheet instabilities. J. Geophys. Res. Earth 126 (4). https://doi.org/10.1029/2020JF005755 e2020JF005755.
Ghienne, J.F., Deynoux, M., 1998. Large scale channel fill structures in Late Ordovician glacial deposits in Mauritania, western Sahara. Sediment. Geol. 119 (1–2), 141–159. https://doi.org/10.1016/S0037-0738(98)00045-1.
Giglio, C., Benetti, S., Sacchetti, F., Lockhart, E., Hughes Clarke, J., Plets, R., Van Landeghem, K., Ó Cofaigh, C., Scourse, J., Dunlop, P., 2021. A Late Pleistocene channelized subglacial meltwater system on the Atlantic continental shelf south of Ireland. Boreas. https://doi.org/10.1111/bor.12536.
Girard, F., Ghienne, J.-F., Rubino, J.-L., Huuse, M., Redfern, J., Heron, D.P.L., Dixon, R. J., Moscariello, A., Craig, J., 2012. Channelized sandstone bodies ('cordons') in the Tassili N'Ajjer (Algeria & Libya): Snapshots of a Late Ordovician proglacial outwash plain. In: Glaciogenic Reservoirs and Hydrocarbon Systems, vol. 368. Geological Society of London, p. 0.
Graham, A.G.C., Lonergan, L., Stoker, M.S., 2007. Evidence for Late Pleistocene ice stream activity in the Witch Ground Basin, central North Sea, from 3D seismic reflection data. Quat. Sci. Rev. 26 (5), 627–643. https://doi.org/10.1016/j.quascirev.2006.11.004.
Graham, A.G.C., Lonergan, L., Stoker, M.S., 2010. Depositional environments and chronology of Late Weichselian glaciation and deglaciation in the central North Sea. Boreas 39, 471–491. https://doi.org/10.1111/j.1502-3885.2010.00144.x.
Hamblin, R.J.O., Moorlock, B.S.P., Rose, J., Lee, J.R., Riding, J.B., Booth, S.J., Pawley, S. M., 2005. Revised Pre-Devensian glacial stratigraphy in Norfolk, England, based on mapping and till provenance. Neth. J. Geosci. 84 (2), 77–85. https://doi.org/10.1017/S0016774600022976.
Hepp, D.A., Hebbeln, D., Kreiter, S., Keil, H., Bathmann, C., Ehlers, J., Mörz, T., 2012. An east-west-trending Quaternary tunnel valley in the South-Eastern North Sea and its seismic-sedimentological interpretation. J. Quat. Sci. 27 (8), 844–853. https://doi.org/10.1002/jqs.2599.
Hirst, J.P.P., Huuse, M., Redfern, J., Heron, D.P.L., Dixon, R.J., Moscariello, A., Craig, J., 2012. Ordovician proglacial sediments in Algeria: insights into the controls on hydrocarbon reservoirs in the In Amenas field, Illizi Basin. In: Glaciogenic Reservoirs and Hydrocarbon Systems, vol. 368. Geological Society of London, p. 0.
Hjelstuen, B.O., Nygård, A., Sejrup, H.P., Haflidason, H., 2012. Quaternary denudation of southern Fennoscandia – evidence from the marine realm. Boreas 41 (3), 379–390. https://doi.org/10.1111/j.1502-3885.2011.00239.x.
Hooke, R.L., Jennings, C.E., 2006. On the formation of the tunnel valleys of the southern Laurentide ice sheet. Quat. Sci. Rev. 25 (11–12), 1364–1372. https://doi.org/10.1016/j.quascirev.2006.01.018.
Huber, C., Leuenberger, M., Spahni, R., Flückiger, J., Schwander, J., Stocker, T.F., Johnsen, S., Landais, A., Jouzel, J., 2006. Isotope calibrated Greenland temperature record over Marine Isotope Stage 3 and its relation to CH4. Earth Planet. Sci. Lett. 243 (3), 504–519. https://doi.org/10.1016/j.epsl.2006.01.002.
Huuse, M., Lykke-Andersen, H., 2000a. Large-scale glaciotectonic thrust structures in the eastern Danish North Sea. Geol. Soc. Lond. Spec. Publ. 176 (1), 293–305. https://doi.org/10.1144/gsl.Sp.2000.176.01.22.
Huuse, M., Lykke-Andersen, H., 2000b. Overdeepened Quaternary valleys in the eastern Danish North Sea morphology and origin. Quat. Sci. Rev. 19, 1233–1253. https://doi.org/10.1016/S0277-3791(99)00103-1.
Huuse, M., Le Heron, D.P., Dixon, R., Redfern, J., Moscariello, A., Craig, J., 2012. Glaciogenic reservoirs and hydrocarbon systems: An introduction. In: Huuse, M., Redfern, J., Le Heron, D.P., Dixon, R.J., Moscariello, A., Craig, J. (Eds.), Glaciogenic Reservoirs and Hydrocarbon Systems, vol. 368. London, Geological Society, Special Publications, pp. 1–28.
Iverson, N., Person, M., 2012. Glacier-bed geomorphic processes and hydrologic conditions relevant to nuclear waste disposal. Geofluids 12 (1), 38–57. https://doi.org/10.1111/j.1468-8123.2011.00355.x.
Janszen, A., Moreau, J., Moscariello, A., Ehlers, J., Kröger, J., 2012a. Time-transgressive tunnel-valley infill revealed by a three-dimensional sedimentary model, Hamburg, north-West Germany. Sedimentology 60 (3), 693–719. https://doi.org/10.1111/j.1365-3091.2012.01357.x.
Janszen, A., Spaak, M., Moscariello, A., 2012b. Effects of the substratum on the formation of glacial tunnel valleys: an example from the Middle Pleistocene of the southern North Sea Basin. Boreas 41 (4), 629–643. https://doi.org/10.1111/j.1502-3885.2012.00260.x.
Jørgensen, F., Sandersen, P.B.E., 2006. Buried and open tunnel valleys in Denmark—erosion beneath multiple ice sheets. Quat. Sci. Rev. 25 (11–12), 1339–1363. https://doi.org/10.1016/j.quascirev.2005.11.006.
Jouzel, J., Masson-Delmotte, V., Cattani, O., Dreyfus, G., Falourd, S., Hoffmann, G., Minster, B., Nouet, J., Barnola, J.M., Chappellaz, J., Fischer, H., Gallet, J.C., Johnsen, S., Leuenberger, M., Loulergue, L., Luethi, D., Oerter, H., Parrenin, F., Raisbeck, G., Raynaud, D., Schilt, A., Schwander, J., Selmo, E., Souchez, R., Spahni, R., Stauffer, B., Steffensen, J.P., Stenni, B., Stocker, T.F., Tison, J.L., Werner, M., Wolff, E.W., 2007. Orbital and millennial antarctic climate variability over the past 800,000 years. Science 317 (5839), 793–796. https://doi.org/10.1126/science.1141038.
Kallweit, R.S., Wood, L.C., 1982. The limits of resolution of zero-phase wavelets. Geophysics 47 (7), 1035–1046. https://doi.org/10.1190/1.1441367.
Karstens, J., Berndt, C., 2015. Seismic chimneys in the Southern Viking Graben – Implications for palaeo fluid migration and overpressure evolution. Earth Planet. Sci. Lett. 412, 88–100. https://doi.org/10.1016/j.epsl.2014.12.017.
Kehew, A.E., Piotrowski, J.A., Jørgensen, F., 2012. Tunnel valleys: concepts and controversies — A review. Earth Sci. Rev. 113 (1–2), 33–58. https://doi.org/10.1016/j.earscirev.2012.02.002.
Kindler, P., Guillevic, M., Baumgartner, M., Schwander, J., Landais, A., Leuenberger, M., 2014. Temperature reconstruction from 10 to 120 kyr b2k from the NGRIP ice core. Clim. Past 10 (2), 887–902. https://doi.org/10.5194/cp-10-887-2014.
King, E.C., 2020. The precision of radar-derived subglacial bed topography: a case study from Pine Island Glacier, Antarctica. Ann. Glaciol. 1-8 https://doi.org/10.1017/aog.2020.33.
King, E.C., Hindmarsh, R.C.A., Stokes, C.R., 2009. Formation of mega-scale glacial lineations observed beneath a West Antarctic ice stream. Nat. Geosci. 2 (8), 585–588. https://doi.org/10.1038/ngeo581.
Kirkham, J.D., Hogan, K.A., Larter, R.D., Self, E., Games, K., Huuse, M., Stewart, M.A., Ottesen, D., Arnold, N.S., Dowdeswell, J.A., 2021. Tunnel valley infill and genesis revealed by high-resolution 3-D seismic data. Geology 49 (12), 1516–1520. https://doi.org/10.1130/g49048.1.
Kirkham, J.D., Hogan, K., Larter, R.D., Arnold, N., Ely, J.C., Self, E., Games, K., Huuse, M., Stewart, M., Ottesen, D., Dowdeswell, J.A., 2022. Tunnel valley formation beneath deglaciating mid-latitude ice sheets: observations and modelling. Quat. Sci. Rev. 323, 107680.
Kluiving, S.J., Bosch, J.A., Ebbing, J.H., Mesdag, C.S., Westerhoff, R.S., 2003. Onshore and offshore seismic and lithostratigraphic analysis of a deeply incised Quaternary buried valley system in the Northern Netherlands. J. Appl. Geophys. 53 (4), 249–271. https://doi.org/10.1016/j.jappgeo.2003.08.002.
Kristensen, T.B., Huuse, M., 2012. Multistage erosion and infill of buried Pleistocene tunnel valleys and associated seismic velocity effects. Geol. Soc. Lond. Spec. Publ. 368 (1), 159–172. https://doi.org/10.1144/sp368.15.
Kristensen, T.B., Huuse, M., Piotrowski, J.A., Clausen, O.R., 2007. A morphometric analysis of tunnel valleys in the eastern North Sea based on 3D seismic data. J. Quat. Sci. 22 (8), 801–815. https://doi.org/10.1002/jqs.1123.
Kristensen, T.B., Piotrowski, J.A., Huuse, M., Clausen, O.R., Hamberg, L., 2008. Time-transgressive tunnel valley formation indicated by infill sediment structure, North Sea – the role of glaciohydraulic supercooling. Earth Surf. Process. Landf. 33 (4), 546–559. https://doi.org/10.1002/esp.1668.
Kuhlmann, G., Wong, T.E., 2008. Pliocene paleoenvironment evolution as interpreted from 3D-seismic data in the southern North Sea, Dutch offshore sector. Mar. Pet. Geol. 25 (2), 173–189. https://doi.org/10.1016/j.marpetgeo.2007.05.009.
Laban, C., 1995. The Pleistocene Glaciations in the Dutch Sector of the North Sea [PhD Unpublished PhD thesis]. University of Amsterdam.
Lamb, R.M., Harding, R., Huuse, M., Stewart, M., Brocklehurst, S.H., 2018. The early Quaternary North Sea Basin. J. Geol. Soc. Lond. 175 (2), 275–290. https://doi.org/10.1144/jgs2017-057.
Lang, J., Winsemann, J., Steinmetz, D., Polom, U., Pollok, L., Böhner, U., Serangeli, J., Brandes, C., Hampel, A., Winghart, S., 2012. The Pleistocene of Schöningen, Germany: a complex tunnel valley fill revealed from 3D subsurface modelling and shear wave seismics. Quat. Sci. Rev. 39, 86–105. https://doi.org/10.1016/j.quascirev.2012.02.009.

Lang, J., Lauer, T., Winsemann, J., 2018. New age constraints for the Saalian glaciation in northern Central Europe: implications for the extent of ice sheets and related proglacial lake systems. Quat. Sci. Rev. 180, 240–259. https://doi.org/10.1016/j.quascirev.2017.11.029.

Lawson, D.E., Strasser, J.C., Evenson, E.B., Alley, R.B., Larson, G.J., Arcone, S.A., 1998. Glaciohydraulic supercooling: a freeze-on mechanism to create stratified, debris-rich basal ice: I. Field evidence. J. Glaciol. 44 (148), 547–562. https://doi.org/10.3189/S0022143000002069.

Le Heron, D.P., Sutcliffe, O., Bourgig, K., Craig, J., Visentin, C., Whittington, R.J., 2004. Sedimentary architecture of Upper Ordovician tunnel valleys, Gargaf Arch, Libya: implications for the genesis of a hydrocarbon reservoir. GeoArabia 9 (2), 137–160.

Lee, J.R., Busschers, F.S., Sejrup, H.P., 2012. Pre-Weichselian Quaternary glaciations of the British Isles, the Netherlands, Norway and adjacent marine areas south of 68°N: implications for long-term ice sheet development in northern Europe. Quat. Sci. Rev. 44, 213–228. https://doi.org/10.1016/j.quascirev.2010.02.027.

Lelandais, T., Ravier, É., Pochat, S., Bourgeois, O., Clark, C., Mourgues, R., Strzerzynski, P., 2018. Modelled subglacial floods and tunnel valleys control the life cycle of transitory ice streams. Cryosphere 12 (8), 2759–2772. https://doi.org/10.5194/tc-12-2759-2018.

Livingstone, S.J., Lewington, E.L.M., Clark, C.D., Storrar, R.D., Sole, A.J., McMartin, I., Dewald, N., Ng, F., 2020. A quasi-annual record of time-transgressive esker formation: implications for ice-sheet reconstruction and subglacial hydrology. Cryosphere 14 (6), 1989–2004. https://doi.org/10.5194/tc-14-1989-2020.

Lohrberg, A., Schwarzer, K., Unverricht, D., Omlin, A., Krastel, S., 2020. Architecture of tunnel valleys in the southeastern North Sea: new insights from high-resolution seismic imaging. J. Quat. Sci. https://doi.org/10.1002/jqs.3244.

Lohrberg, A., Schneider von Deimling, J., Grob, H., Lenz, K.F., Krastel, S., 2022. Tunnel valleys in the southeastern North Sea: more data, more complexity. E&G Q. Sci. J. 71 (2), 267–274. https://doi.org/10.5194/egqsj-71-267-2022.

Lonergan, L., Maidment, S.C.R., Collier, J.S., 2006. Pleistocene subglacial tunnel valleys in the Central North Sea basin: 3-D morphology and evolution. J. Quat. Sci. 21 (8), 891–903. https://doi.org/10.1002/jqs.1015.

Løseth, H., Dowdeswell, J.A., Batchelor, C.L., Ottesen, D., 2020. 3D sedimentary architecture showing the inception of an Ice Age. Nat. Commun. 11 (1), 2975. https://doi.org/10.1038/s41467-020-16776-7.

Løseth, H., Nygård, A., Batchelor, C.L., Fayzullaev, T., 2022. A regionally consistent 3D seismic-stratigraphic framework and age model for the Quaternary sediments of the northern North Sea. Mar. Pet. Geol. 142, 105766 https://doi.org/10.1016/j.marpetgeo.2022.105766.

Lüthi, D., Le Floch, M., Bereiter, B., Blunier, T., Barnola, J.-M., Siegenthaler, U., Raynaud, D., Jouzel, J., Fischer, H., Kawamura, K., Stocker, T.F., 2008. High-resolution carbon dioxide concentration record 650,000–800,000 years before present. Nature 453 (7193), 379–382. https://doi.org/10.1038/nature06949.

Montelli, A., Dowdeswell, J.A., Pirogova, A., Terekhina, Y., Tokarev, M., Rybin, N., Martyn, A., Khoshtariya, V., 2020. Deep and extensive meltwater system beneath the former Eurasian Ice Sheet in the Kara Sea. Geology 48, 179–183. https://doi.org/10.1130/g46968.1.

Moreau, J., Huuse, M., 2014. Infill of tunnel valleys associated with landward-flowing ice sheets: the missing Middle Pleistocene record of the NW European rivers? Geochem. Geophys. Geosyst. 15 (1), 1–9. https://doi.org/10.1002/2013gc005007.

Mugford, R.I., Dowdeswell, J.A., 2011. Modeling glacial meltwater plume dynamics and sedimentation in high-latitude fjords. J. Geophys. Res. Earth 116 (F1). https://doi.org/10.1029/2010JF001735.

Müther, D., Back, S., Reuning, L., Kukla, P., Lehmkuhl, F., 2012. Middle Pleistocene landforms in the Danish Sector of the southern North Sea imaged on 3D seismic data. In: Huuse, M., Redfern, J., Le Heron, D.P., Dixon, R.J., Moscariello, A., Craig, J. (Eds.), Glaciogenic Reservoirs and Hydrocarbon Systems, vol. 368. Geological Society, Special Publications, London, pp. 111–127.

Nygård, A., Sejrup, H.P., Haflidason, H., Bryn, P., 2005. The glacial North Sea Fan, southern Norwegian Margin: architecture and evolution from the upper continental slope to the deep-sea basin. Mar. Pet. Geol. 22 (1), 71–84. https://doi.org/10.1016/j.marpetgeo.2004.12.001.

Ó Cofaigh, C., 1996. Tunnel valley genesis. Prog. Phys. Geogr. 20 (1), 1–19. https://doi.org/10.1177/030913339602000101.

Ottesen, D., Rise, L., Andersen, E.S., Bugge, T., Eidvin, T., 2009. Geological evolution of the Norwegian continental shelf between 61°N and 68°N during the last 3 million years. Nor. J. Geol. 89, 251–265.

Ottesen, D., Dowdeswell, J.A., Bugge, T., 2014. Morphology, sedimentary infill and depositional environments of the Early Quaternary North Sea Basin (56°–62°N). Mar. Pet. Geol. 56, 123–146. https://doi.org/10.1016/j.marpetgeo.2014.04.007.

Ottesen, D., Stokes, C.R., Bøe, R., Rise, L., Longva, O., Thorsnes, T., Olesen, O., Bugge, T., Lepland, A., Hestvik, O.B., 2016. Landform assemblages and sedimentary processes along the Norwegian Channel Ice Stream. Sediment. Geol. 338, 115–137. https://doi.org/10.1016/j.sedgeo.2016.01.024.

Ottesen, D., Batchelor, C.L., Dowdeswell, J.A., Løseth, H., 2018. Morphology and pattern of Quaternary sedimentation in the North Sea Basin (52–62°N). Mar. Pet. Geol. 98, 836–859. https://doi.org/10.1016/j.marpetgeo.2018.08.022.

Ottesen, D., Stewart, M., Brönner, M., Batchelor, C.L., 2020. Tunnel valleys of the central and northern North Sea (56°N to 62°N): distribution and characteristics. Mar. Geol. 425 https://doi.org/10.1016/j.margeo.2020.106199.

Passchier, S., Laban, C., Mesdag, C.S., Rijsdijk, K.F., 2010. Subglacial bed conditions during Late Pleistocene glaciations and their impact on ice dynamics in the southern North Sea. Boreas. https://doi.org/10.1111/j.1502-3885.2009.00138.x.

Pawley, S.M., Bailey, R.M., Rose, J., Moorlock, B.S.P., Hamblin, R.J.O., Booth, S.J., Lee, J.R., 2008. Age limits on Middle Pleistocene glacial sediments from OSL dating, North Norfolk, UK. Quat. Sci. Rev. 27 (13), 1363–1377. https://doi.org/10.1016/j.quascirev.2008.02.013.

PGS, 2020. CNS MegaSurveyPlus, vol. 2020. PGS. https://www.pgs.com/data-library/europe/nw-europe/north-sea/cns/.

Piotrowski, J.A., 1997. Subglacial hydrology in North-Western Germany during the last glaciation: groundwater flow, tunnel valleys and hydrological cycles. Quat. Sci. Rev. 16, 169–185. https://doi.org/10.1016/S0277-3791(96)00046-7.

Praeg, D., 1996. Morphology, Stratigraphy and Genesis of Buried Mid-Pleistocene Tunnel Valleys in the Southern North Sea Basin. PhD thesis. University of Edinburgh.

Praeg, D., 2003. Seismic imaging of mid-Pleistocene tunnel-valleys in the North Sea Basin—high resolution from low frequencies. J. Appl. Geophys. 53 (4), 273–298. https://doi.org/10.1016/j.jappgeo.2003.08.001.

Raza, A., Gholami, R., Rezaee, R., Rasouli, V., Rabiei, M., 2019. Significant aspects of carbon capture and storage – A review. Petroleum 5 (4), 335–340. https://doi.org/10.1016/j.petlm.2018.12.007.

Rea, B.R., Newton, A.M.W., Lamb, R.M., Hardling, R., Bigg, G.R., Rose, P., Spagnolo, M., Huuse, M., Cater, J.M.L., Archer, S., Buckley, F., Halliyeva, M., Huuse, J., Cornwell, D.G., Brocklehurst, S.H., Howell, J., 2018. Extensive marine terminating ice sheets in Europe from 2.5 million years ago. Sci. Adv. 4 (6) https://doi.org/10.1126/sciadv.aar8327 eaar8327.

Rose, J., 2009. Early and Middle Pleistocene landscapes of eastern England. Proc. Geol. Assoc. 120 (1), 3–33. https://doi.org/10.1016/j.pgeola.2009.05.003.

Rose, P., Byerley, G., Vaughan, O., Cater, J., Rea, B.R., Spagnolo, M., Archer, S., 2018. Aviat: a Lower Pleistocene shallow gas hazard developed as a fuel gas supply for the Forties Field. Geol. Soc. Lond. Petrol. Geol. Conf. Ser. 8 (1), 485–505. https://doi.org/10.1144/pgc8.16.

Roskosch, J., Winsemann, J., Polom, U., Brandes, C., Tsukamoto, S., Weitkamp, A., Bartholomäus, W.A., Henningsen, D., Frechen, M., 2015. Luminescence dating of ice-marginal deposits in northern Germany: evidence for repeated glaciations during the Middle Pleistocene (MIS 12 to MIS 6). Boreas 44 (1), 103–126. https://doi.org/10.1111/bor.12083.

Sandersen, P.B.E., Jørgensen, F., Larsen, N.K., Westergaard, J.H., Auken, E., 2009. Rapid tunnel-valley formation beneath the receding Late Weichselian ice sheet in Vendsyssel, Denmark. Boreas 38 (4), 834–851. https://doi.org/10.1111/j.1502-3885.2009.00105.x.

Sejrup, H.P., Haflidason, H., Aarseth, I., King, E., Forsberg, C.F., Long, D., Rokoengen, K., 1994. Late Weichselian glaciation history of the northern North Sea. Boreas 23 (1), 1–13. https://doi.org/10.1111/j.1502-3885.1994.tb00581.x.

Sejrup, H.P., Aarseth, I., Haflidason, H., Løvlie, R., Bratten, Å., Tjøstheim, G., Forsberg, C.F., Ellingsen, K.L., 1995. Quaternary of the Norwegian Channel: glaciation history and palaeoceanography. Nor. Geol. Tidsskr. 75 (2–3), 65–87.

Serov, P., Vadakkepuliyambatta, S., Mienert, J., Patton, H., Portnov, A., Silyakova, A., Panieri, G., Carroll Michael, L., Carroll, J., Andreassen, K., Hubbard, A., 2017. Postglacial response of Arctic Ocean gas hydrates to climatic amelioration. Proc. Natl. Acad. Sci. 114 (24), 6215–6220. https://doi.org/10.1073/pnas.1619288114.

Severinghaus, J.P., Brook, E.J., 1999. Abrupt climate change at the end of the last glacial period inferred from trapped air in polar ice. Science 286 (5441), 930–934. https://doi.org/10.1126/science.286.5441.930.

Sharp, M., 1985. Sedimentation and stratigraphy at Eyjabakkajökull—an icelandic surging glacier. Quat. Res. 24 (3), 268–284. https://doi.org/10.1016/0033-5894(85)90050-X.

Sharpe, D., Dyke, L., Hinton, M., Pullan, S., Russell, H., Brennand, T., Barnett, P., Pugin, A., 1996. Groundwater prospects in the Oak Ridges Moraine area, southern Ontario: application of regional geological models. Curr. Ther. Res. 1996, 181–190.

Shreve, R.L., 1972. Movement of water in glaciers. J. Glaciol. 11 (62), 205–214. https://doi.org/10.3189/S002214300002219X.

Solheim, A., Pfirman, S.L., 1985. Sea-floor morphology outside a grounded, surging glacier; Bråsvellbreen, Svalbard. Mar. Geol. 65, 127–143. https://doi.org/10.1016/0025-3227(85)90050-7.

Steinmetz, D., Winsemann, J., Brandes, C., Siemon, B., Ullmann, A., Wiederhold, H., Meyer, U., 2015. Towards an improved geological interpretation of airborne electromagnetic data: a case study from the Cuxhaven tunnel valley and its Neogene host sediments (Northwest Germany). Neth. J. Geosci. 94 (2), 201–227. https://doi.org/10.1017/njg.2014.39.

Stewart, M.A., 2009. 3D Seismic Analysis of Pleistocene Tunnel Valleys in the Central North Sea [Unpublished PhD Thesis Unpublished PhD Thesis]. Imperial College London, 317 p.

Stewart, M.A., Lonergan, L., 2011. Seven glacial cycles in the middle-late Pleistocene of Northwest Europe: geomorphic evidence from buried tunnel valleys. Geology 39 (3), 283–286. https://doi.org/10.1130/g31631.1.

Stewart, M., Lonergan, L., Hampson, G., 2012. 3D seismic analysis of buried tunnel valleys in the Central North Sea: Tunnel valley fill sedimentary architecture. In: Huuse, M., Redfern, J., Le Heron, D.P., Dixon, R., Moscariello, A., Craig, J. (Eds.), Glaciogenic Reservoirs and Hydrocrabon Systems, vol. 368. Geological Society, London, Special Publications, pp. 173–184.

Stewart, M.A., Lonergan, L., Hampson, G., 2013. 3D seismic analysis of buried tunnel valleys in the Central North Sea: morphology, cross-cutting generations and glacial history. Quat. Sci. Rev. 72, 1–17. https://doi.org/10.1016/j.quascirev.2013.03.016.

Stoker, M.S., Skinner, A.C., Fyfe, J.A., Long, D., 1983. Palaeomagnetic evidence for early Pleistocene in the central and northern North Sea. Nature 304, 332–334. https://doi.org/10.1038/304332a0.

Stoker, M.S., Balson, P.S., Long, D., Tappin, D., 2011 (Year) Published An overview of the lithostratigraphical framework for the Quaternary deposits on the United Kingdom continental shelf.

Storrar, R.D., Stokes, C.R., Evans, D.J.A., 2014. Morphometry and pattern of a large sample (>20,000) of Canadian eskers and implications for subglacial drainage

beneath ice sheets. Quat. Sci. Rev. 105, 1–25. https://doi.org/10.1016/j.quascirev.2014.09.013.
Storrar, R.D., Ewertowski, M., Tomczyk, A.M., Barr, I.D., Livingstone, S.J., Ruffell, A., Stoker, B.J., Evans, D.J.A., 2019. Equifinality and preservation potential of complex eskers. Boreas. https://doi.org/10.1111/bor.12414.
Syvitski, J.P.M., 1989. On the deposition of sediment within glacier-influenced fjords: Oceanographic controls. Mar. Geol. 85 (2), 301–329. https://doi.org/10.1016/0025-3227(89)90158-8.
van der Vegt, P., Janszen, A., Moscariello, A., 2012. Tunnel valleys: Current knowledge and future perspectives. In: Huuse, M., Redfern, J., Le Heron, D.P., Dixon, R., Moscariello, A., Craig, J. (Eds.), Glaciogenic Reservoirs and Hydrocarbon Systems, vol. 368. Geological Society, Special Publications, London, pp. 75–97.
Vandenberghe, J., 2000. A global perspective of the European chronostratigraphy for the past 650ka. Quat. Sci. Rev. 19 (17), 1701–1707. https://doi.org/10.1016/S0277-3791(00)00096-2.
von Berlepsch, T., Haverkamp, B., 2016. Salt as a host rock for the geological repository for nuclear waste. Elements 12 (4), 257–262. https://doi.org/10.2113/gselements.12.4.257.
Waite, W.F., Santamarina, J.C., Cortes, D.D., Dugan, B., Espinoza, D.N., Germaine, J., Jang, J., Jung, J.W., Kneafsey, T.J., Shin, H., Soga, K., Winters, W.J., Yun, T.-S., 2009. Physical properties of hydrate-bearing sediments. Rev. Geophys. 47 (4) https://doi.org/10.1029/2008RG000279.
Warwel, A., Hübscher, C., Ahlrichs, N., Schnabel, M., 2022. New insights into tunnel valley locations and Cenozoic exhumation in the southwestern Baltic Sea based on Machine Learning aided seismic refraction tomography. Mar. Geophys. Res. 43 (3), 35. https://doi.org/10.1007/s11001-022-09492-y.
Wingfield, R., 1989. Glacial incisions indiciating Middle and Upper Pleistocene ice limits off Britain. Terra Nova 1, 538–548. https://doi.org/10.1111/j.1365-3121.1989.tb00430.x.
Wingfield, R., 1990. The origin of major incisions within the Pleistocene deposits of the North Sea. Mar. Geol. 91 (1–2), 31–52. https://doi.org/10.1016/0025-3227(90)90131-3.
Winsborrow, M., Andreassen, K., Hubbard, A., Plaza-Faverola, A., Gudlaugsson, E., Patton, H., 2016. Regulation of ice stream flow through subglacial formation of gas hydrates. Nat. Geosci. 9 (5), 370–374. https://doi.org/10.1038/ngeo2696.
Winsemann, J., Koopmann, H., Tanner, D.C., Lutz, R., Lang, J., Brandes, C., Gaedicke, C., 2020. Seismic interpretation and structural restoration of the Heligoland glaciotectonic thrust-fault complex: Implications for multiple deformation during (pre-)Elsterian to Warthian ice advances into the southern North Sea Basin. Quat. Sci. Rev. 227, 106068 https://doi.org/10.1016/j.quascirev.2019.106068.
Winters, W.J., Pecher, I.A., Waite, W.F., Mason, D.H., 2004. Physical properties and rock physics models of sediment containing natural and laboratory-formed methane gas hydrate. Am. Mineral. 89 (8–9), 1221–1227. https://doi.org/10.2138/am-2004-8-909.
Ziegler, P.A., 1990. Geological Atals of Western and Central Europe. Geological Society, London.
Ziegler, P.A., 1992. North Sea rift system. Tectonophysics 208, 55–75. https://doi.org/10.1016/0040-1951(92)90336-5.